HIGH TEMPERATURE DEFORMATION MECHANISMS IN SUPERPLASTIC ZINC-ALUMINIUM (22 w% Al) EUTECTOID ALLOY

A Thesis Submitted
In Partial Fulfilment of the Requirements
for the Degree of
DOCTOR OF PHILOSOPHY

BY
MADHUSUDAN LAXMAN VAIDYA

to the

DEPARTMENT OF METALLURGICAL ENGINEERING
INDIAN INSTITUTE OF TECHNOLOGY KANPUR

FEBRUARY 1972

CERTIFICATE

This is to certify that this work "HIGH TEMPERATURE DEFORMATION MECHANISMS IN SUPERPLASTIC ZINC-ALUMINIUM (22w% Al) EUTECTOID ALLOY", has been carried out by Mr. Madhusudan Laxman Vaidya under my supervision, and it has not been submitted elsewhere for a degree.

G.S. Murty

G.S. MURTY
Assistant Professor
Department of Metallurgical Engineering
Kanpur, India

ACKNOWLEDGEMENTS

I take this opportunity to thank sincerely Dr. G.S. Murty and Late Professor J.E. Dorn who provided superb guidance and general supervision throughout the course of the present work. I am very much indebted to both of them.

Special thanks are due to Dr. K.L. Murty of Lawrence Berkeley Laboratories, California (USA), who helped me in conducting the creep experiments and offered useful suggestions and critical comments.

Thanks are due to Dean E.C. Subbarao and Professor K.P. Gupta whose help facilitated me to complete the major part of the work at the Department of Material Science and Engineering, Berkeley, California (USA). They provided encouragement throughout the course of my Ph.D. programme.

Grateful acknowledgements are due to Kanpur Indo-American Program for providing training facilities in U.S.A.

Mr. M. Natu and Mr. N. Ahmad are to be congratulated and thanked for excellent typing. Mr. Prithipal Singh is thanked for his help in preparing drawings.

Last but not the least, my heartfelt thanks to my wife, Mangala, whose patience and encouragement saw me through this work.

TABLE OF CONTENTS

LIST OF TABLES

LIST OF FIGURES

LIST OF SYMBOLS

T	-	Absolute temperature in °Kelvin
T_m	-	Absolute temperature of melting expressed in °kelvin
μ_m	-	micron (10^{-4} cm)
σ	-	Tensile true stress
K	-	Constant
k	-	Boltzman constant
$\dot{\varepsilon}$	-	Tensile true strain rate
m	-	Strain-rate sensitivity index
d	-	Grain diameter
L	-	Grain diameter (=d)
ΔH	-	Activation energy
R	-	Gas constant
ε_o	-	Constant
n	-	Stress exponent (a constant)
A	-	Constant
X	-	X( ), a function of stress
A_i	-	Pre-exponential factor for an ith process
S	-	Entropy factor
s	-	Structure factor
ΔH_i	-	Activation energy for the ith process
A'	-	Constant, independent of stress and temperature.

B	-	Constant
α	-	Constant $= \frac{B}{n}$ (also used for Al-rich solid solution)
S'	-	Universal creep constant for pure metals.
ω	-	Grain boundary with
r	-	Thermal recovery rate
h	-	$\frac{d\gamma}{dt}$ where γ = true shear strain and t = time
$\dot{\varepsilon}_s$	-	Strain rate due to Grain Boundary sliding
a	-	Constant
β	-	Constant (also used for Zn-rich solid solution)
σ_o	-	Back-stress (Tensile)
B_3	-	Constant
U	-	Activation energy for grain boundary diffusion
η	-	Constant
c	-	Constant
Q	-	Activation energy
A''	-	Constant.
D	-	Diffusivity in cm^2/sec
E	-	Young's modulus
D_o	-	Diffusion constant
G	-	Shear modulus of material
b	-	Burgers vector
A_c	-	Constant
m'	-	Constant

N - True strain exponent = constant

K' - Constant

K'' - Constant

D_v - Volume diffusivity

A_n - Constant

D^* - Tracer diffusivity

N_A - Atomic fraction of element A

N_B - Atomic fraction of element B

D_g - $D_g b$ = Grain boundary diffusivity

A_n' - Constant

A_g' - Constant

n' - Constant

V_k - Viscous flow rate

Q_k - Activation energy for viscous flow

V_b - Grain boundary sliding velocity

Q_b - Activation energy for grain boundary sliding

$'$ - Geometrical constant

Ω - Atomic volume

$A'_g b$ - Constant

A_d - Constant

g - Constant

τ - True shear stress

$\dot{\gamma}$ - True shear strain rate

SYNOPSIS

In order to understand the role of such atomistic processes as diffusional flow of vacancies, grain boundary sliding and dislocation climb and glide, during the deformation of superplastic alloys, under the temperature and strain rate ranges where superplasticity is exhibited, a detailed investigation has been undertaken on Zinc-Aluminium (22w% Al) eutectoid alloy. The part played by each of these processes in the deformation of Zn-Al eutectoid is not clearly understood since there have been some serious contradictions in the experimental observations[1-5] reported in the literature regarding stress (τ) - strain rate ($\dot{\gamma}$) relationship, grain size influence on $\tau(\dot{\gamma})$ and activation energies involved in the deformation over various strain-rate ranges.

Very fine grained structure ($<10\mu$) - a necessary concomitant for the superplasticity - has been obtained by quenching hot rolled samples from 375°C to 0°C. Variation in grain size, from 1.8 to 5.5μ, has been achieved by annealing treatment given to the quenched samples at 265°C for various periods.

Experimental data on stress-strain rate has been obtained, covering a strain-rate range of 10^{-8} to 1 per second ($\sim$8 cycles), at about 250°C (0.68 Tm). Creep tests have been performed to obtain data at very low strain rates viz., 10^{-8} to 10^{-4} per second. Instron tests have been used to obtained data covering strain rate range of 10^{-5} to 1 per second. Shear test specimens have been used to avoid any complications due to change in the specimen cross-section and strain rate with increasing strain during the deformation.

From the log ($\dot{\gamma}$) vs log (τ) plots for various grain sizes, three regions (I, II and III) have been clearly delineated in the particular alloy. Region I is characterised by a slope of $\sim$1, region II by a slope of $\sim$2 and region III by a slope of $\sim$3.5. The extent of each region varies with the grain size. The grain size dependence of strain rate in region I is 3, in region II is 2 and nearly independent in the region III.

Activation energies obtained from the plots of log ($\dot{\gamma}$) vs ($\frac{1}{T}$) for various regions indicate a value of $\sim$16.2 Kcal/mole for region I, $\sim$16.27 Kcal/mole for the region II and $\sim$27.43 Kcal/mole for the region III.

The activation energy in region I compares favourably

with the activation energy value for grain boundary self diffusion of Zn. Also the $\dot{\gamma}(\tau)$ data and grain size dependence of strain rate compares very well with the theoretical predictions by Coble[6] creep model. It is, therefore, concluded that Coble mechanism, involving diffusional flow of matter via grain boundaries is the controlling mechanism in the region I. Consistent with the mechanism, at small strains, very little microstructural changes have been observed.

In the region II, grain boundary sliding mechanism has been proposed as the rate controlling process accompanied by dislocation climb as a process of accommodation. This conclusion has been based on the fact that the present data is best explained by an existing model[5] incorporating grain boundary sliding as a controlling process aided by grain boundary diffusion controlled dislocation climb. Rounding off of grain corners and equiaxed grain structure has been observed microscopically which is consistent with the model.

The region III is controlled by viscous glide motion of dislocation, as proposed by Weertman[7]. This conclusion is based on the observed strain rate dependence of ~ 3.5 on stress, and the activation energy close to the volume self diffusion energy of zinc. The microstructural changes involving grain elongation have been observed and it is consistent with the controlling mechanism.

CHAPTER - 1

INTRODUCTION

Studies on mechanical behaviour of metals at high temperatures are important from the standpoint of their applicability and formability. The former is usually measured in terms of creep resistance and the latter in terms of ductility (% elongation). Besides these macroscopic aspects there is a microscopic aspect to these studies, namely, the atomistic mechanisms controlling the deformation behaviour. Understanding the atomistic mechanisms is a problem of fundamental importance.

A group of two-phase and a few single-phase alloys have been found to possess remarkable ductility over certain strain rates and at high temperatures ($\geqslant 0.5$ Tm). The unique ability of these materials to deform plastically with fluid like character of hot polymers and glasses has earned them a name 'superplastic' materials. In solid crystalline materials this is a relatively rare phenomenon. The unusual ductility effects were noted[1] as far back as in 1920 but only in recent five to six years large number of investigations have been carried out with a specific purpose of knowing the important factors controlling the superplastic behaviour

and to commercially exploit the property. To a small group of two or three alloys, now, are added as many as 35 (see Appendix I) different alloys including both single and two-phase alloys. Two-phase Zinc-Aluminium eutectoid is one of the prominent superplastic alloys.

It is now commonly accepted that superplasticity in Zn-Al eutectoid and similar other superplastic alloys is closely associated with the aggregates of extremely small (of the order of 1 to 10μm) size. There is a certain range of strain rates over which only, the behaviour is noticeable. The micro-structure, unlike in other cases, does not alter but remains equiaxed.

Phenomenologically, superplastic behaviour is shown[2] to be a direct consequence of high strain rate sensitivity of these fine grained materials at temperatures greater than approximately 0.5 Tm, where Tm is absolute melting temperature. In an equation, $\sigma = K\dot{\varepsilon}^m$, where σ is tensile stress $\dot{\varepsilon}$ is tensile strain rate and K and m are constants, the strain rate sensitivity index 'm' assumes values $\geqslant 0.5$ in the superplastic behaviour. In the usual plastic behaviour at temperatures above 0.5 Tm the value of m lies below 0.2.

In spite of the large number of studies, it is not

yet clear, however, which atomistic mechanisms predominate in these materials under superplastic conditions. Many well established high temperature mechanisms, namely, stress directed vacancy flow, grain boundary sliding (GBS), dynamic recovery, have been invoked to explain the behaviour but none of them has been accepted universally. There are conflicting claims as to the part played by each of the established basic mechanisms. Further experimentation is needed in that connection.

In order that definitive conclusions regarding mechanism could be drawn there is a need to obtain accurate data on the stress dependence of strain rates over a wide range of values. Different strain rate regions could then be delineated depending upon the slopes (m values) on the log-log plot of stress vs strain rates over various strain-rate ranges. The stress-strain rate dependence in various regions could then be compared with those given by different well established atomistic theories. Further, since the high temperature behaviour is thermally activated, activation energies need to be determined accurately and compared with those of the existing mechanisms such as volume diffusion, grain boundary diffusion etc. Finally,

metallographic observations should be consistent with the proposed mechanisms.

Zinc-Aluminium eutectoid is one of the most studied amongst the two-phase alloys. On close scrutiny of the existing data[2-6] on the system, it is revealed that there are conflicting claims regarding the dependence of 'm' on strain rate. Some workers have shown that 'm' varies continuously with strain rate. It attains a peak value of 0.5 at some intermediate strain rate and tapers off to lower values on both the sides of the peak (Figure 1). Whereas, some have shown that 'm' consistently approaches a specific value (0.5) over a considerable range (2-3 orders) of strain rate (Figure 2) indicating predominance of one single mechanism over a large strain rate. Further, the data on stress-strain rate at very low strain rates is very scanty and unrealiable because of ambiguities in the experimental procedures. This adds to the difficulty of evaluating the mechanisms.

The activation energies for deformation are not well established in Zn-Al eutectoid. The reported values fall into two groups, one where same value is observed as in conventional creep by dislocation climb (activation

energy for lattice self diffusion), the other where the value is lower and can be identified with grain boundary self diffusion.

The analysis presented in the literature is not clear as to the degree of grain size dependence of strain rate at constant stress and temperature. The dependence varies from $d^{-0.7}$ to d^{-2}. There are experimental difficulties in determining 'd' and its exact meaning for two-phase materials.

In the reanalysis of the Zinc-Aluminium data by Bird, Mukherjee and Dorn[7] (Figure 3) in the context of their review on correlation between high temperature creep behaviour and structure they have indicated a definite possibility of coble creep-mechanism predominating at lower stress levels in the system. They do not envision superplastic behaviour as a transition region controlled by two or more mechanisms but a distinct region with a 'm' value of ~ 0.5. These conclusions are drawn by comparison of the superplastic behaviour with the existing creep theories.

The present work on Zn-Al eutectoid has thus originated in (i) the conflicting claims regarding the

temperature, grain size and stress dependence of strain rates, (ii) the lack of unambiguous data below strain rate of 10^{-5} per min, and (iii) the reanalysis of the Zn-Al data by Bird, Mukherjee and Dorn[7].

The objectives of the investigation were:

1. To obtain extensive stree-strain rate data from very low to fairly high strain rates using constant stress creep tests for lower strain rates and instron tests for the higher ones.
2. Double shear specimen were to be used to overcome the probable errors introduced by nonuniform deformation in the compression creep tests and changing cross-section in tensile creep tests.
3. To determine activation energies in the various strain rate regions.
4. To determine accurately the grain size dependence of stress-strain rate relationship.
5. To note the metallographic changes over various regions of stress-strain rates.
6. Finally, to correlate the data in terms of the various theoretical models proposed for steady state deformation at high temperatures and propose modification, if any.

CHAPTER - 2

MECHANICAL BEHAVIOUR OF METALS AT HIGH TEMPERATURES

Mechanical behaviour of metals at elevated temperatures is controlled primarily by thermally activated processes. That is, the strength and ductility of metals at such high temperatures are strongly dependent on strain rate and temperature. Strain-hardening is eliminated at these temperatures because recovery processes predominate and the behaviour of the metals is characterized by its 'creep' strength or resistance. It is, therefore, relevant for the present work to understand some basic aspects of creep of metals.

Creep behaviour of materials is described by a creep test. In this test a constant load or a constant stress is applied and the change in material dimensions is recorded as a function of time. Two important variables influencing creep behaviour are temperature and stress. Such other variables as structure, elastic modulus and stacking fault energy also influence the behaviour.

2.1 CREEP OF PURE METALS

A typical high temperature creep curve shows

called 'flowability') against the reciprocal of the absolute temperature, he pointed out that one obtains at constant stress, a negative slope equal to $\frac{\Delta H}{R}$ where ΔH represents a value for the energy of steady state creep and R is the gas constant. According to Kanter

$$\ln\left(\frac{f_T}{f_o}\right) = -\frac{\Delta H}{RT} \qquad (2.1)$$

where F_T is the flowability at temperature T and f_o is a constant. He derived a mathematical expression which is identical to an empirical relation proposed by Dorn[9], namely,

$$\dot{\varepsilon} = \varepsilon_o \sigma^n \exp\left(-\frac{\Delta H}{RT}\right) \qquad (2.2)$$

where ε_o is a constant and n is stress exponent.

The early identification of creep as a thermally activated process led Kauzmann[10] and Dushman et al.[11] to apply the principles of reaction rate theory to the analysis of creep data. According to them creep rate is given by

$$\dot{\varepsilon} = AT\exp\left(-\frac{\Delta H}{RT}\right) \sin h\left(\frac{X}{RT}\right) \qquad (2.3)$$

where A is an independent constant and $X = X(\sigma)$, a function of applied stress.

In terms of the characteristics temperature dependence of the experimental observations and from the theoretical work supporting these evidences, the creep deformation has been shown to be the result of one or more thermally activated atomic mechanisms. For a given thermally activated mechanism of creep, the steady state creep rate $\dot{\varepsilon}$, is represented in the most general form as

$$\dot{\varepsilon} = A_i (\sigma, T, S, s) \exp \left\{ - \frac{\Delta Hi (\sigma, T, s)}{RT} \right\} \qquad (2.4)$$

where A_i is the pre-exponential factor frequently called the frequency factor which is, in general, a function of the applied stress (σ), test temperature (T), entropy (S) and structure factor (s); ΔHi is the activation energy for that particular mechanism which could be a function of the stress, temperature and structure.

It is possible that more than one mechanism gives rise to the experimentally observed overall deformation rate. In such multimechanism cases many ΔH's may be involved so that experimentally a weighted average value may be obtained.

2.3 STRESS DEPENDENCE OF STEADY-STATE CREEP RATE

Dorn[9] suggested that the stress dependence of the

creep rate may be identified by the equation,

$$\dot{\varepsilon} = A' (S,s)\ f(\sigma)\ \exp\left\{-\frac{\Delta H}{RT}\right\} \qquad (2.5)$$

where A' is now independent of stress and temperature and that activation energy is not a function of stress and temperature. The above equation has been shown to successfully represent the creep behaviour of many metals over wide ranges of temperature and applied stress. The stress function $f(\sigma)$ seems to take the following forms, depending upon the stress level.

1. $f(\sigma) = \sigma$ at low stresses
2. $f(\sigma) = \sigma^n$ at intermediate stresses
3. $f(\sigma) = \exp(B\sigma)$ at high stresses.

The stress dependence of intermediate and high stress can be replaced by single stress law of the general form

$$f(\sigma) = \sin h\ (B\sigma) \qquad (2.6)$$

Garofalo[12] proposed a similar empirical relationship defining the stress dependence of the steady-state creep rate in metals. Accerding tc him

$$\dot{\varepsilon} = A\ (\sin h\ \alpha\sigma)^n \qquad (2.7)$$

where $\alpha = \frac{B}{n}$ so that

at low stresses $\dot{\varepsilon} \sim \sigma^n$ (2.8)

at high stresses $\dot{\varepsilon} \sim \exp(B\sigma)$ (2.9)

It has been shown by Sherby[13] in his comprehensive article on the factors affecting the high temperature strength of poly crystalline solids that the general expression for creep of pure metals might be given by

$$\dot{\varepsilon} = S' L^2 D \left(\frac{\sigma}{E}\right)^5 \qquad (2.10)$$

where L is the grain diameter in cm, S' is a universal constant for all pure metals with a value of about 10^{29} cm^{-4}, D is the diffusion coefficient in cm^2/sec and E is the Young's modulus of the material. Here the modulus compensated stress seems to be a more fundamental parameter than simple stress.

In a recent survey by Bird, Mukherjee and Dorn[7], it has been shown that many aspects of high temperature steady state creep at moderate stresses can be correlated by semiempirical equation.

$$\frac{\dot{\varepsilon} kT}{DGb} = Ac \left(\frac{\sigma}{G}\right)^n \qquad (2.11)$$

where Ac and n are dimensionless quantities (constants), k is the Boltzman's constant, D is the diffusivity

(equal to Do exp $-\frac{\Delta H}{kT}$), G is the shear modulus of the material and b is burger's vector.

For fine grained material the same expression assumes the form

$$\frac{\dot{\varepsilon} kT}{DGb} = Ac \left(\frac{b}{d}\right)^{m'} \left(\frac{\sigma}{G}\right)^{n} \qquad (2.12)$$

where d is grain diameter and m' is a constant.

2.4 EXPERIMENTAL OBSERVATIONS OF ACTIVATION ENERGIES FOR CREEP OF METALS

Determination of the activation energies for deformation to identify the underlying rate controlling mechanism has been extensively used in recent times. All activation energy data was compiled by Dorn[14], Sherby et al.[15], Conrad[16], and by Garofalo[12]. These include the data for the deformation behaviour over the whole range of temperatures. These compilations show that at temperatures above about half the melting point expressed in absolute units and under moderate stresses (not too high), many materials exhibit apparent activation energies for steady state creep nearly equal to that for self diffusion. These activation energies are called 'apparent activation energies' by Dorn because it will be possible to measure

the true activation energies for deformation at high temperatures until exact mechanism is known. Nevertheless, since the results indicate no significant difference between these values and those for self diffusion, these apparent activation energies approximate to the true activation energies for the deformation.

2.5 DETERMINATION OF ACTIVATION ENERGY FOR DEFORMATION

It has been shown before that the creep behaviour of a metal can be described implicitly by a rate equation of the form

$$\dot{\varepsilon} = A\,(\sigma,\ T,\ S,\ s)\ \exp\ -\frac{\Delta H\ (\sigma,\ T,\ S)}{RT} \qquad (2.13)$$

If a single mechanism controls the overall creep rate, the activation energy for creep by that mechanism is given by

$$\Delta H = -R\,\frac{\partial \ln \dot{\varepsilon}}{\partial \left(\frac{1}{T}\right)} \qquad (2.14)$$

the pre-exponential factor (A) being regarded as independent of the temperature. This assumption is permissible since A has a very weak temperature dependence.

Experimental techniques leading to determination of the observed activation energies are given in Appendix II.

2.6 MECHANICAL STABILITY DURING CREEP DEFORMATION

A ductile material when stretched by a tensile force can deform uniformly only while stable flow occurs. The limit of stable flow is marked by the onset of geometrical instability. That is, after a certain uniform extension, deformation suddenly concentrates at a given point and ceases elsewhere. Such instability produces the commonly observed regions of localized deformation (necks) which eventually lead to rupture. The necking phenomenon occurs irrespective of temperature but the controlling factors differ with temperature. At temperature below 0.3 Tm instability occurs when the material has exhausted its capacity for strain hardening and the true strain ε at this point is shown (Appendix III) to be numerically equal to the strain hardening index N, defined in the expression

$$\sigma = K'\varepsilon^{N} \qquad (2.15)$$

where σ is the stress and K' is a constant. For further stable extension, the material must be unloaded and then softened, thus restoring the ability to strain harden again on re-applying the load.

If a material does not strain harden there is no uniform elongation, yet at temperatures above half the melting point, where strain hardening effects are less significant, materials often exhibit a considerable range of uniform deformation and sometimes quite high elongations result. In these circumstances, therefore, some factor other than strain hardening must control the ability to flow in a stable manner. Above 0.5 Tm, where equilibrium between recovery and hardening exhists[17] the important parameter is strain rate sensitivity (S.R.S.) and this replaces the strain hardening index N which is the controlling factor at low temperatures. The magnitude of the SRS is of considerable importance in most cases of superplastic deformation.

Rossard's[18] treatment of mechanical stability during creep deformation assumes that a mechanical equation of state exists with the form

$$\sigma = K'' \varepsilon^{N} \dot{\varepsilon}^{m} \qquad (2.16)$$

where $\dot{\varepsilon}$ is the strain rate and m is the index of S.R.S. Assuming N constant, Rossard showed theoretically that stable flow is possible provided $m \geqslant \frac{1}{2}$ for constant

velocity testing and $m \geq 1/3$ for constant strain rate testing. In creep terminology this means that the stress exponent should not be > 2 for stable deformation. A more rigorous analysis due to Hart[19] confirms these conclusions.

CHAPTER - 3

HIGH TEMPERATURE DEFORMATION MECHANISMS

There are many well established high temperature structural mechanisms proposed in the context of high temperature steady state creep phenomenon and hot working processes. Some of them have been invoked to explain the superplastic behaviour by various workers. It is, therefore, pertinent to know details about the relevant mechanisms.

These mechanisms could be classified into two groups: (i) those operative at low stresses and (ii) those operative at high stresses. Diffusion plays an important role in most of them.

The various low stress high temperature diffusion controlled mechanisms that have been identified are:

Atomic transport processes : (1) Nabarro-herring mechanism

(2) Coble mechanism

Dislocation-motion based processes:

(1) Climb mechanism

(2) Viscous glide mechanism

Grain-boundary sliding mechanisms:

(1) Gifkin's model

(2) Langdon's model

The various high stress mechanisms that have been identified are:

Dynamic Recovery process

Dynamic Recrystallization process.

3.1 ATOMIC TRANSPORT PROCESSES

At sufficiently high temperatures ($\geqslant 0.5\ T_m$) and low stresses crystalline solids can deform at a significant rate by atomic transport processes. This phenomenon is possible because there exists, in real crystalline materials, locations where atoms can be added to, or removed from, the crystal lattice. When the material is stress free, and in equilibrium, the chemical potentials at these sinks and sources are everywhere the same, but on application of a stress, providing that is not purely hydrostatic, chemical differences arise. These provide a driving force for diffusion between sources and sinks, and the resultant transport of matter changes the shape of the material in response to the deforming forces. The sources and sinks for atoms may be free surfaces, grain boundaries

or dislocations, while diffusion paths may be through the lattice, through a vapor phase, along a free surface, along grain boundaries or along dislocation cores.

3.1.1 Nabarro-Herring Creep Mechanism[20,21]

Nabarro-Herring postulated that the creep results from the diffusion of vacancies from the regions of high chemical potential at grain boundaries subjected to normal tensile stresses to regions of lower chemical potential where the average tensile stresses across the grain boundaries are zero (Figure 5). Atoms migrating in the opposite direction through the lattice account for the creep strain. When the volume diffusion controls the steady state tensile creep rate, , is given by

$$\dot{\varepsilon} = A_n \frac{D_v b^3 \sigma}{d^2 kT} \qquad (3.1)$$

where b is the burger's vector, σ is the applied stress, d is the mean grain diameter and kT is the Boltzmann constant times the absolute temperature. A_n is a constant. The diffusivity D_v, is obtained from the tracer diffusivity D^*. For pure metals

$$D_v = \frac{D^*}{f} \qquad (3.2)$$

and for binary solution

$$D_v = \frac{D_A^* \, D_B^*}{(N_A \, D_A^* + N_B \, D_B^*) f} \qquad (3.3)$$

where N_A and N_B are the atomic fractions of A and B atoms, and f is the correlation factor. The dimensionless constant A_n depends insensitively on the geometry of grains, but is generally estimated to have a value from 8 to 5.

Nabarro creep does not invoke the motion of dislocation. It predominates over high temperature dislocation dependent mechanisms only at low stress levels and then, only for fine grained materials.

In order to provide a ready comparison of Nabarro creep with other mechanisms to be discussed later, the equation (3.1) is reformulated as

$$\frac{\dot{\varepsilon} \, kT}{D_v G b} = A_n \left(\frac{b}{d}\right)^2 \left(\frac{\sigma}{G}\right)^1 \qquad (3.4)$$

where G is the shear modulus of elasticity.

3.1.2 Coble Creep Mechanism[22]

Coble creep results from the diffusion of vacancies from regions of high chemical potential at grain boundaries

subjected to normal tensile stresses to regions of lower chemical potential where average tensile stress across the grain boundaries is zero. Atoms migrate via grain boundaries instead of migrating through the lattice as in the case of Nabarro creep. The creep is given by an expression similar to that for Nabarro creep except for the grain size dependence. The equation as reformulated is

$$\frac{\dot{\varepsilon}\, kT}{D_{gb} Gb} = A_n' \left(\frac{b}{d}\right)^3 \left(\frac{\sigma}{G}\right)^1 \qquad (3.5)$$

where D_{gb} is the grain boundary diffusivity and A_n' is a constant which depends insensitively on the geometry of grains and estimated[7] to have value of 48.

The grain boundary diffusion mechanism should predominate over volume diffusion when

$$48 \left(\frac{b}{d}\right) \left(\frac{D_{gb}}{D_v}\right) > 7 \qquad (3.6)$$

3.1.3 General Remarks on Atomic Transport Processes

A number of experiments confirming N–H creep by volume diffusion has been reported (Pranatis and Pound[23], Greenough[24], Hondros[25]). Until recently, the diffusional flow processes were considered to be of only academic interest, being confined to temperatures within a few

degrees of the melting point. However, there are two effects which extend the range to temperatures of engineering application. First, a dispersion of second phase particles can so inhibit dislocation movement that lattice diffusion creep becomes the dominant deformation mode at least down to 0.7 T_m. Secondly, the occurrence of grain boundary diffusion can produce viscous flow in fine grained materials at temperatures $\lesssim 0.6\ T_m$. Jones[26] has reported Coble creep in Mg and Bernstein[27] has reported it in Zr. It has been reported in several ceramic oxides too[28].

In recent years, it has been shown through detailed analysis by Liftshitz[29] and later by Gibbs[30] that for coherent deformation of polycrystalline aggregates by pure diffusional flow of atoms, grain boundary sliding is an essential concomitant. This follows from the following arguments. If any arbitrary region of a polycrystalline aggregate is capable of undergoing a general shape change, the local strain tensor must have six independent components. A constant volume boundary condition reduces this number to five. Diffusion can given five independent strain components for an individual grain, but acting alone it would lead to discontinuities in the strain-tensor

at grain boundary triple points. Diffusion creep of a polycrystalline aggregate, therefore, requires simultaneous operation of some other accommodation process to maintain coherency. Since dislocation slip cannot occur at such stress levels, grain boundary sliding must occur to preserve the continuity (sliding which occurs solely for this reason does not contribute additional specimen extension). If, for some reason, grain boundary sliding is impossible, then the material can deform only by diffusion current between free surfaces. The creep rates, in that case, would be extremely small.

In 1963, Harris et al.[31], contrary to earlier belief, observed inhibition of diffusional creep by second phase particles. Two possible reasons are suggested for this phenomenon: (i) the prevention of necessary grain boundary sliding due to a layer of second phase particle accumulating at the grain boundaries, or (ii) the lowering of the efficiency of vacancy generation or absorption by the second phase particles.

Gibbs[32] has argued that, if particles can inhibit sliding sufficiently, it may become the rate controlling process. However, this should give d^{-1} dependence of

$$\frac{\dot{\varepsilon} kT}{D_v Gb} = A_c \left(\frac{\sigma}{G}\right)^n \qquad (3.7)$$

where A_c and n are dimensionless quantities and the diffusivity D_v is given by equations (3.2) and (3.3), n generally ranges in value from 4.2 to 7. A_c is estimated to be approximately 2.5×10^6.

3.2.2 Dislocation Glide Controlled Creep

Weertman[35] proposed a creep mechanism for solid solution alloys based on the following dislocation model. Dislocation loops are assumed to be created at Frank-Read sources. They move out from a source at a velocity controlled by either micro-creep mechanism or Pierls stress mechanism. After moving a distance L the dislocation are annihilated by climbing to dislocations of opposite sign which are created from sources on neighbouring slip planes. The time required for climb is assumed to be so short that the climb process is not rate controlling. The steady state creep rate for low stresses is given by

$$\frac{\dot{\varepsilon} kT}{D_v Gb} = A'_g \left(\frac{\sigma}{G}\right)^{n'} \qquad (3.8)$$

where n takes values from 3 to 3.5. A'_g is estimated to be 5×10^{-1}.

3.3 GRAIN-BOUNDARY SLIDING

Observations have established that three distinctly different types of grain boundary sliding occur. When sliding is limited to submicroscopic regions of a boundary, as in damping capacity-experiments, one kind of behaviour is observed. When sliding occurs over a relatively long length of boundary but is unconstrained by adjacent grains, as in bicrystals, another type of behaviour results. Yet a third type is obtained when sliding occurs in polycrystalline aggregates, where continuity conditions exert considerable control over the sliding process.

Damping capacity experiments show[36] that local microscopic grain boundary sliding obeys a Newtonian viscosity flow

$$V_k = A_k \sigma \exp\left(-\frac{Q_k}{RT}\right) \qquad (3.9)$$

such that V_k increases linearly with σ and has an activation energy Q_k which equals that for volume diffusion.

In contrast, grain boundary sliding and grain boundary zone sliding in bicrystals may give sliding rate[7]

3.3 GRAIN-BOUNDARY SLIDING

Observations have established that three distinctly different types of grain boundary sliding occur. When sliding is limited to submicroscopic regions of a boundary, as in damping capacity-experiments, one kind of behaviour is observed. When sliding occurs over a relatively long length of boundary but is unconstrained by adjacent grains, as in bicrystals, another type of behaviour results. Yet a third type is obtained when sliding occurs in polycrystalline aggregates, where continuity conditions exert considerable control over the sliding process.

Damping capacity experiments show[36] that local microscopic grain boundary sliding obeys a Newtonian viscosity flow

$$V_k = A_k \sigma \exp\left(-\frac{Q_k}{RT}\right) \qquad (3.9)$$

such that V_k increases linearly with σ and has an activation energy Q_k which equals that for volume diffusion.

In contrast, grain boundary sliding and grain boundary zone sliding in bicrystals may give sliding rate[7]

$$V_b = A_b \sigma^2 \exp\left(-\frac{Q_b}{RT}\right) \qquad (3.10)$$

where the stress squared term arises from stress concentrations and Q_b is the activation energy for grain boundary diffusion.

The velocities of shear displacement are yet orders of magnitude lower in polycrystalline aggregates than across grain boundaries in bicrystals. Obviously, additional constraints to grain boundary sliding are encountered in polycrystalline aggregates. These arise principally from the need to maintain continuity over boundary rough spots and at triple points.

3.3.1 Gifkin's Model

Gifkin and Snowden[37] proposed a diffusion controlled mechanism for GBS creep, based on the movement of double ledges or protrusions along boundary. The suggestion is that the sliding along the interledge section of the boundary is permitted to occur at the rate at which longest protrusion (see Figure 7) moves by diffusion of atoms from one protrusion to the other. The driving force for the diffusion arises from stress concentrated on the ledge sliding between them. The strain rate is given by

$$\frac{\dot{\varepsilon} kT}{D_{gb} Gb} = \alpha' \Omega \left(\frac{\sigma}{G}\right)^1 \left(\frac{b}{d}\right)^1 \qquad (3.11)$$

where α' is a geometrical constant, approximately equal to 2, Ω is the atomic volume, d is the length of the protrusion. Gifkin[38] has modified the above expression to take care of the triple point accommodation. The strain rate expression is

$$\frac{\dot{\varepsilon} kT}{D_{gb} Gb} = 40 \Omega \omega \left(\frac{\sigma}{G}\right) \left(\frac{b}{d}\right)^1 \qquad (3.12)$$

where ω is grain boundary width and d is grain diameter.

3.3.2 Langdon's Model

Using transmission electron microscopy, it has been shown that there are only a few isolated dislocations in, or immediately adjacent to, the grain boundaries of an annealed but unstrained polycrystal, but that the dislocation content increases rapidly with increasing strain (Hale, Ishida, Lin, McLean, 1966)[39]. It is not immediately clear whether these dislocations come into the boundaries from the lattice or are formed in the boundary and thence move into the grains; whilst both processes probably occur, present evidence suggests that they primarily originate within the grains and

enter the boundary region by slip (Lin and McLean, 1968)[40].

Such dislocations appear to retain their crystallographic Burgers vectors and sliding is, therefore, possible if they move along the boundary by alternate climb and glide (ishida and Henderson, Brown, 1967)[41] so that shear displacement arises from the component of the Burgers vector parallel to the boundary. Basing his arguments on these observations, Langden[42] has put forth a model for creep by GBS. He assumes that GBS is controlled by the rate of climb of dislocations visualized as one of the steps in the process. The strain rate is given by

$$\dot{\varepsilon} = \beta \frac{b^2\sigma^2}{dGkT} D_v \qquad (3.13)$$

where β is a constant close to unity. In the reformulated form the expression is

$$\frac{\dot{\varepsilon} kT}{D_v Gb} = A'_{gb} \left(\frac{\sigma}{G}\right)^2 \left(\frac{b}{d}\right)^1 \qquad (3.14)$$

where A'_{gb} is a constant.

3.3.3 General Remarks on GBS

Gibbs[43] has argued that GBS would never control deformation at very low stresses. At higher stresses

where dislocation motion predominates over diffusional flux, GBS could control the deformation if the crystal structure offers less than five independent slip systems as in case of close packed hexagonal structure. GBS alone can provide only two independent strain components (in the plane of the boundary) in the localized regions. It must, therefore, always be accompanied by other deformation processes within the grain.

3.4 DYNAMIC RECOVERY AND RECRYSTALLIZATION

When strain free grains are produced by recovery/ recrystallization all signs of prior hardening are removed and ductility is restored. Thus, by careful cold working, with sufficient intermediate anneals, it is possible to produce extensive stable deformation. It would appear reasonable, therefore, to invoke a continuous version of such a process, i.e., deformation with simultaneous annealing to account for superplasticity.

Cottrell and Aytekin[44] and Mott[45] introduced a creep theory incorporating both work hardening and recovery. The theory is often called 'recovery theory'. In the proposal, it is assumed that steady state occurs when the rate 'r' of thermal recovery - $(\partial \tau_i / \partial t)_{\dot{\gamma}} = 0$

Table - I

Mechanism	Strain rate Expression	Remarks
Nabarro-Herring	$\frac{\dot{\varepsilon} kT}{D_v Gb} = A_n (\frac{\sigma}{G})^1 (\frac{b}{d})^2$	
Coble	$\frac{\dot{\varepsilon} kT}{D_{gb} Gb} = A'_n (\frac{\sigma}{G})^1 (\frac{b}{d})^2$	
Dislocation Climb	$\frac{\dot{\varepsilon} kT}{D_v Gb} = A_c (\frac{\sigma}{G})^n (\frac{b}{d})^o$	$n \simeq 4$
Dislocation Glide	$\frac{\dot{\varepsilon} kT}{D_v Gb} = A'_g (\frac{\sigma}{G})^{n'} (\frac{b}{d})^o$	$n \simeq 3$ to 3.5
Gifkin	$\frac{\dot{\varepsilon} kT}{D_{gb} Gb} = A_{gb} (\frac{\sigma}{G})^1 (\frac{b}{d})^2$	
Langdon	$\frac{\dot{\varepsilon} kT}{D_v Gb} = A'_{gb} (\frac{\sigma}{G})^2 (\frac{b}{d})^1$	
Recovery	$\dot{\varepsilon} = \frac{A'_d}{h'} \exp \left[- \frac{(\Delta H_i - q'\sigma)}{RT} \right]$	

equals the rate of hardening $(\partial\tau_i/\partial t)\, r = 0$ where τ_i is the internal shear stress (due to working). If the rate of recovery is given by

$$\left(\frac{\partial \tau_i}{t}\right) \dot{\gamma} = o = - A_d \exp \left[\frac{-(\Delta H_i - q\tau)}{RT} \right] \qquad (3.15)$$

where A_d and q are constants, $\dot{\gamma}$ is shear strain rate, τ is equivalent to the mean internal stress or the yield stress, and the rate of hardening is given by

$$\left(\frac{\partial \tau_i}{t}\right) r = o = \frac{d\gamma}{dt} \left(\frac{\partial \tau_i}{\partial \gamma}\right) r = o = \frac{d\gamma}{dt}\, h = - \left(\frac{\partial \tau_i}{\partial t}\right) \dot{\gamma} = o$$

then for steady state

$$\dot{\gamma}_s = \frac{A_d}{h} \exp \left[\frac{-(\Delta H_i - q\tau)}{RT} \right] \qquad (3.16)$$

an equivalent expression for tensile strain rate would be

$$\dot{\varepsilon} = \frac{A'_d}{h'} \exp \left[- \frac{(\Delta H_i - q'\sigma)}{RT} \right]$$

where A'_d, q' are constants $h' = \left(\frac{\partial \sigma_i}{\partial \varepsilon}\right)$, σ_i being internal stress.

3.5 SUMMARY

The important features of each mechanism mentioned earlier are tabulated in Table (I). It would be clear that dynamic recovery mechanism does not involve grain size dependence of strain rate explicitly. Also the activation energy factor is very much stress dependent.

more remarkable, upon pulling at temperature near 275°C, elongations upto 450% were measured. Structural metastability was broadly identified as a condition for such behaviour although the details of any relationships were not very closely specified. Much less concern was shown for the extensive stretchability except calling it 'superplasticity'.

Backofen et al.[22] were the first to concern themselves with the unusual tensile ductility of the Zn-Al eutectoid. They argued that in the absence of strain hardening at temperatures above 0.5 T_m, the superplastic behaviour could be explained in terms of increased strain-rate sensitivity (SRS). To verify their explanations, they evaluated the SRS over a wide range of strain rates (10^{-3} per min. to 1 per min.) through instantaneous pulling speed changes. They showed that the superplastic behaviour (% elongations as high as 1000%) corresponded with the strain rate sensitivity values > 0.3.

The results of Backofen et al's experiments[2] (Figure 9) indicate that 'm' - the SRS index - varies continuously with strain-rate and temperature. The

more remarkable, upon pulling at temperature near 275°C, elongations upto 450% were measured. Structural metastability was broadly identified as a condition for such behaviour although the details of any relationships were not very closely specified. Much less concern was shown for the extensive stretchability except calling it 'superplasticity'.

Backofen et al.[22] were the first to concern themselves with the unusual tensile ductility of the Zn-Al eutectoid. They argued that in the absence of strain hardening at temperatures above 0.5 T_m, the superplastic behaviour could be explained in terms of increased strain-rate sensitivity (SRS). To verify their explanations, they evaluated the SRS over a wide range of strain rates (10^{-3} per min. to 1 per min.) through instantaneous pulling speed changes. They showed that the superplastic behaviour (% elongations as high as 1000%) corresponded with the strain rate sensitivity values > 0.3.

The results of Backofen et al's experiments[2] (Figure 9) indicate that 'm' - the SRS index - varies continuously with strain-rate and temperature. The

stress vs strain rate data (Figure 10) has not been plotted clearly on log-log scale to clearly differentiate the slope of the curve into various regions. The curves do not indicate any sigmoidal behaviour.

At the time when Backofen et al. reported their results on Zn-Al system, they did not propose any definitive structural mechanism for superplastic deformation. However, they suggested that the deformation is Bingham[53] type and diffusion controlled.

The phenomenological importance of SRS shown by Backofen et al. in Zn-Al alloy led to similar studies on other superplastic alloys, e.g., Pb-Sn[54], Al-Cu[55] eutectics, etc. No significant work was reported on Zn-Al system until 1967 when Alden[4], Holt[3] and Chaudhuri[5] reported their findings separately. Holt[3] investigated the relationship between grain boundary sliding and the superplastic behaviour. He was primarily checking a previous proposal that the high strain rate sensitivity, characterizing the superplastic deformation, is the combined result of extensive boundary sliding and migration processes. Holt used compression specimen in Instron machine to measure 'm' as a function of

strain rate in the same manner as suggested by Backofen et al. The Instron tests covered a strain rate range of 4×10^{-3} to 4×10^{1} per minute. A gas operated testing machine was used to obtain data at higher strain rates ($>4\times10^{1}$ per min.). To obtain data at strain rate $<4\times10^{-3}$ per minute creep tests were carried out by compressing specimen by constant load. Creep strain rate was measured as an average value computed by dividing strain at the end of the test by loading time. Metallographic technique was used to measure the contribution of grain boundary shear to total strain.

Metallographic measurements indicated that, at 250°C, $\dot{\varepsilon}_s/\dot{\varepsilon}$, where $\dot{\varepsilon}_s$ is strain rate due to GBS and $\dot{\varepsilon}$ is the total strain rate, was low at both high and low strain rates but reaches a maximum, estimated as 60% at an intermediate rate of 5×10^{-3} per min. There was a wide scatter in the results. Rate sensitivity, as measured by 'm', followed the same trend as $\dot{\varepsilon}_s/\dot{\varepsilon}$ vs. strain rate - the maximum occurring at approximately the same strain rate in both the cases.

Log-log plots for σ vs. $\dot{\varepsilon}$, for various grain sizes and at 250°C, from Holt's data (Figure 11) indicate

trends towards sigmoidal nature of the plot as in case of Pb-Sn eutectic alloy. The variation of 'm' with strain rate was found to be continously (Figure 12) changing. The stress, σ vs. grain size L, at different constant strain rates- cross plots from σ vs. $\dot{\varepsilon}$ curves- indicated that in an expression $\sigma \propto L^{a}$, 'a' varies from 0.7 at $\dot{\varepsilon} = 10^{-4}$/min. to 1.2 at $\dot{\varepsilon} = 10^{-1}$/min. Above 5×10^{2}/min. strain rate, grain size dependence on strain rate was negligible.

From Holt's results it is clear that grain boundary sliding plays an very significant role over a certain range of strain rates. As for the data on σ vs. $\dot{\varepsilon}$, the accuracy of the results is very much questionable for two reasons: (i) the inhomogeneous deformation of the test specimen (bulging) during testing, (ii) the crude way of determining the strain rates during creep testing. Further, there is room to believe - for want of specific observation otherwise - that structure (grain size) would have changed during the creep period affecting the strain rates. This is so because the annealing temperature prior to testing and the test temperature for creep tests are the same, viz.,

At almost the same period as Holt (1967), Chaudhuri[5] reported the findings of his work on the Zn-Al eutectoid system. He carried out tensile creep tests on the alloy and measured the temperature dependence of the steady state strain rate in terms of activation energies over a wide range of temperatures. He found that the activation energy was temperature dependent; the values of 35.3 ± 1.0 Kcal/g. atom and 21.0 ± 1.0 Kcal/g.atom, for temperatures of deformation above 200°C and below 175°C respectively, were reported. Further, his results indicated that the temperature compensated strain rate *vs*, stress plot had constant slope over a wide range of strain rates (Figure 13) indicating that SRS (or 'm') could be constant over a range of strain rates. He showed that 'm' was dependent on grain size. Grain growth was reported during creep deformation, making the results of stress *vs*. strain rate of questionable validity. His experiments had the same drawback as those of Holt - of not stabilizing the grain size at higher annealing temperature than the one used for testing. However, the constancy of 'm' over a wide range of strain rates was of considerable importance from the standpoint of mechanism. X-ray

and metallographic evidence by Chaudhari showed that the two phases in the Zn-Al eutectoid remain equiaxed even after considerable deformation in the so-called superplastic range. No preferred orientation was developed.

Nearly at the same time when Chaudhari reported his findings, Alden[4] also reported the findings on the system (Figure 14). The log-log plot of σ vs. $\dot{\varepsilon}$ shows a considerable region of nearly same slope of ~0.5. The slope varied little with the grain size. No sigmoidal nature was reported; instead the log-log plot of $\sigma(\dot{\varepsilon})$ shows definite trends towards higher 'm' values at lower strain rates (Figure 15).

In spite of the extensive work on various superplastic systems, there was no agreed theory to explain the structural basis of the superplastic behaviour. Ball-Hutchison[6], just like Alden[4], argued that the maximum observed value of 'm', at temperatures just below the eutectoid or eutectic temperatures, consistently approached 0.5. Therefore, there should be a distinct mechanism operating during the superplastic deformation. To confirm the values of 'm' they conducted tensile tests in the Instron machine on Zn-Al eutectoid. Optical

and electron microscopic studies of the structural changes were also carried out. Following were the important results:

Stress (σ) vs. Temperature (T) - at constant strain rate:

An approximately linear relationship between $\log\sigma$ and $\frac{1}{T}$ (Figure 16) exists; the slopes of the curves are independent of grain size.

Stress vs. Strain-rate

The variation of $\log\sigma$ with $\log\dot{\varepsilon}$ is linear at lower strain rates but curves over at higher rates (Figure 18). The slope of the linear region approaches 0.5. The slope is constant over a wide range of strain rates and is independent of grain size.

Stress vs. Grain Size (L) - at constant strain rate

A linear relationship exists and the slope of 1 is approached (Figure 17).

The activation energy, as measured from the slope of $\log\sigma$ vs. $\frac{1}{T}$ plots, was found to be $\sim$0.67 eV ($\sim$16 Kcal/mol) in the region of slope $\sim$0.5 on $\log\sigma$ vs. $\log\dot{\varepsilon}$. The value is close to the activation energies for grain boundary diffusion in Zinc ($\sim$0.63 eV) and Al ($\sim$0.73 eV), estimated by taking half the bulk self-diffusion values.

The results on log stress vs. log strain rate closely indicate an extensive region of strain rates over which 'm' remains nearly ($\sim$0.5) constant. The nature of the curve is not sigmoidal. However, there is not enough data below $\dot{\varepsilon}$ of 10^{-4}/min. to clearly indicate any trends. Further significant fact is that there is very little change of 'm' with temperature.

There is an apparent conflict between the results of Ball and Hutchison and Alden on the one side and those of Holt and Backofen on the other. It clearly indicates a need to reinvestigate the Zn-Al eutectoid system and resolve the conflicting claims. Especially, data at lower strain rates need to be obtained to clearly indicate the trends in $\log \bar{\sigma}$ vs. $\log \dot{\varepsilon}$. These, in turn, would throw a light on the mechanisms underlying the deformation of Zn-Al eutectoid. It is also necessary to resolve the conflicting claims about the activation values over various strain rate regions. It would act as a confirmatory test on the mechanisms of deformation.

CHAPTER - 5

THEORETICAL MODELS FOR SUPERPLASTIC BEHAVIOUR

In order to understand the conclusions, drawn from the present investigations, regarding the mechanisms controlling the behaviour of Zn-Al eutectoid at high temperatures, it would be proper to examine the theoretical models proposed to explain the superplastic behaviour of Zn-Al and other similar alloys.

There are several models proposed to explain the structural basis of superplasticity. All of them agree over one fact that the deformation is thermally activated and diffusion plays an important role. The theories can also be categorized into three groups, viz.,

(i) theories based on Diffusional flow of vacancies

(ii) theories based on Grain boundary sliding

(iii) theories based on Dynamic recovery process.

5.1 GROUP I - THEORIES BASED ON DIFFUSIONAL FLOW OF VACANCIES

Avery and Backofen[54] suggested a multimechanism process which combined Nabarro Creep and Dislocation climb controlled creep - both controlled by diffusional flow of vacancies. They argued that the strain rate was a combined

result of both the creep mechanisms; Nabarro creep predominating at lower stresses and dislocation climb creep at the higher stresses. The creep rate, in that case, was given by

$$\dot{\varepsilon} = \frac{A\sigma}{d^2} + B \sinh \beta\sigma \qquad (5.1)$$

where A, B and β are constants; A containing the activation term. Here the first term represents Nabarro creep mechanism and the second term refers to climb controlled creep.

There is a poor agreement between the experimental strain rates and the theoretical rates calculated from the equation (5.1) given by Backofen et al. Actual rates are much higher than the predicted. Further, the expression predicts 'm' value of unity at low strain rates; however, Backofen et al's data indicated a value of 0.4 for 'm' at lower stresses.

In order to overcome the objections put by sigmoidal nature of the log σ vs. log $\dot{\varepsilon}$ plots, Avery and Backofen[55] and others[56,57] suggested further modification to their equation (5.1). They introduced a term called effective stress, $(\sigma-\sigma_o)$, where σ_o was the back stress, replacing 'σ' from the equation (5.1) by $(\sigma-\sigma_o)$ term.

At the present state of undetstanding, the origin of σ_o is only speculative. Only recently it has been recognized by Lifshitz[29], Gibbs[30] and Harris[31] that in order to maintain specimen coherency polycrystals deforming by diffusional flow must necessarily be accompanied by GBS. This would suggest that σ_o may be related to the low rate sensitivity grain boundary resistance.

Avery and Stuart[58] have proposed mechanical fibring at the boundaries preventing sliding to take place to accommodate the deformation produced by diffusional flow. However, they have no evidence for fibring.

Further, it nas been currently proposed[59] that GBS is controlled by the movements of special grain boundary dislocations (GBD) just like the lattice dislocations. Now, for the movement of GBDs, one can imagine a characteristic threshold stress, called 'boundary flow stress' just like the one for lattice dislocations. This boundary flow stress below which sliding cannot occur by grain boundary dislocation movement may give rise to σ_o.

Jones and Johnson[60] replaced the first term in the equation (5.1) by that for Coble mechanism expression. The reformulated expression was

$$\dot{\varepsilon} = \frac{A'\sigma}{d^3} + B \sinh \beta\sigma \qquad (5.2)$$

There was in improved agreement at lower stresses, between experimental values and those calculated from the equation (5.2). However, the objection for 'm' at lower stresses remained.

Packer and Sherby[61] obtained further improvement between strain rates as calculated and those obtained experimentally over the entire range of stress levels by substituting the second term in the equation (5.1) by Weertman's creep rate equation, suggesting Weertman mechanism (viz., viscous glide) controlling the flow at higher stresses and Coble mechanism operating at lower stresses. The modified equation was

$$\dot{\varepsilon} = \frac{A'\sigma}{d^3} + B' \sinh \beta'\sigma^{2.5} \qquad (5.3)$$

All these expressions for the strain rate indicate clearly that vacancy migration creep is a dominant mechanism in the deformation behaviour of Zn-Al or other superplastic alloys. This is specially true at lower stresses and it is highly probable that the rate controlling deformation mechanism in materials with the characteristic fine grained structure would be either lattice or grain boundary diffusion.

Any back stress phenomenon may be a transitional behaviour.

5.2 GROUP II - THEORIES BASED ON GRAIN BOUNDARY SLIDING (GBS)

Gifkin[38] was the first to propose a model based on GBS. According to him the strain rate over the superplastic region was given by

$$\dot{\varepsilon} = B_3 \frac{\sigma\Omega}{kT} D_{gb} \qquad (5.4)$$

where $B_3 = \frac{\text{constant}}{d^3}$. The expression gives a d^{-3} dependence and a stress dependence of unity of the strain rate which conflicts with some of the observations.

Ball and Hutchison[6] proposed a model where the strain rate was mainly given by GBS where dislocation-climb controlled mechanism acted as an accommodation process. They argued that groups of suitably aligned grain slide over each other. Certain grains that obstruct the easy relative motion yield under resulting stress concentration. Under superplastic conditions, dislocations traverse such yielded grains and pile up at grain boundaries until their back stress prevents the boundary sliding. The high stress at the head of the pile up causes accelerated diffusion and dislocations rapidly escape by climb into and along grain boundaries. The strain rate is given by an expression

$$\dot{\varepsilon} = \frac{K\sigma^2}{d^2} \exp\left[-U/kT\right] \qquad (5.5)$$

where U = activation energy for grain boundary diffusion and K is a constant.

Mukherjee[62] has given an expression, based on GBS as the principal mode of deformation, similar to that derived by Ball and Hutchison. The only difference is the value of constant K. Whereas Ball and Hutchison give a value of 50 to 100, Mukherjee gives value of 2. The other difference is that the neighbouring grains need not have to slide as groups as envisioned in Ball and Hutchison model.

Alden[63] has proposed a qualitative model based on GBS and dislocation climb controlled creep. There it is suggested that superplasticity occurs while changing the deformation behaviour from GBS controlled mechanism to dislocation-climb controlled process. Hart[64] proposed a model, supporting Alden, in terms of continuum mechanics. However, it does not explain grain size dependence of $\sigma(\dot{\varepsilon})$ relationship and the spread of superplastic region over a wide strain rate range, as reported by Ball and Hutchison.

5.3. GROUP III - THEORIES BASED ON DYNAMIC RECOVERY

Investigations which indicate that the superplastic

state involves process of continuous recovery have been mainly qualitative and rely chiefly on metallographic evidence. Hyden[65] proposed that Mott's expression for recovery creep analysis,

$$\dot{\varepsilon} = \frac{A'_d}{h} \exp\left[-\frac{(\Delta H_i - q\sigma)}{RT}\right] \qquad (5.6)$$

applies to superplastic behaviour. However, this does not satisfy all the factors involved in the experimental observations.

A continuous recovery mechanism and a relation between stress and strain rate similar to equation (5.1) was proposed by Packer[66] in which the first term is replaced by $\frac{A\sigma^2}{d^3}$ exp $(-\eta/\sigma)$. The factor $\{\exp(-\eta/\sigma)\}$ where η is a constant, is indicated to decrease the efficiency or extent of the recrystallization process at low stress where the energy input is low. It is not clear in what manner the term $\{\exp(-\eta/\sigma)\}$ reflects the fraction of the material recrystallizing. And it is very difficult to see recovery operating at such low strain rates.

Johnson et al.[67] evolved a model combining intergranular deformation (perhaps GBS) followed by recrystallization. Three objections cast doubts about this model. First, there is no periodic fluctuation in the flow stress during the superplastic flow as would be expected if

repeated recrystallization occurred. Secondly, in high temperature creep under thermal and mechanical conditions similar to those required for superplastic deformation no recrystallozation takes place. Thirdly, no recrystallization is seen during the direct observation of superplastic flow[68].

5.4 MODEL BASED ON DISLOCATION MECHANICS

Chaudhari[5] proposed a model based on an analysis of dislocation mechanics in which dislocation velocity is controlled by the motion of jogged screw dislocations and an expression is derived having the form

$$\sigma = B \exp\left(\frac{aQ}{RT}\right) \dot{\varepsilon}^{a} + C \exp\left(\frac{cQ}{RT}\right) \dot{\varepsilon}^{c} \qquad (5.7)$$

where B and C are functions of grain size, and a and c have values of 0.17 - 0.20 and 0.46 - 0.50, respectively, the last constant being identified with conventional SRS (m) at strain rates of the order of 10^{-4} sec^{-1}, where superplastic flow was observed. At slower strain rates flow is non-superplastic and the first term in the equation predominates. The validity of this model is questionable since it is not consistent with the metallographic observations of negligible changes under superplastic conditions.

5.5 GENERAL REMARKS ON THEORIES

The cases for the individual models are equivocal. Nevertheless the bulk of the evidence suggests that grain boundaries are the significant structural elements. Large amounts of GBS have been observed experimentally both directly and indirectly - as a result of grain boundary displacements. Furthermore, direct evidence has been provided that there is considerable diffusion in the boundaries during superplastic deformation and Morrison has shown that alloying elements which enhance diffusion also enhance superplastic behaviour.

It is reasonable to suggest that superplastic deformation is more closely related to creep because of relatively low stresses and low rates of straining as compared to those in Hot working. Recovery models cannot be brought into consideration to explain the behaviour. Coble creep[22] should play an important role in the deformation.

In the recent analysis of the data on Zn-Al eutectoid and Pb-Sn eutectic alloys by Bird, Mukherjee and Dorn[7], it was indicated that strain rates could be more satisfactorily correlated with σ^2 and d^{-2} during the superplastic region of deformation. Such a correlation suggested that

the strain rate could be given by (expression similar to those on creep)

$$\frac{\dot{\varepsilon} kT}{D_{gb} Gb} = K' (\sigma/G)^2 (b/d)^2 \qquad (5.8)$$

reemphasizing the importance of grain boundary diffusion. The equation is essentially the same as that given by Ball and Hutchison[6]. Coble mechanism[22] is proposed to operate at very low strain rates which appears to be highly probable than any back-stress formulation.

CHAPTER - 6

EXPERIMENTAL PROCEDURE

6.1 MATERIALS PREPARATION

Zinc and Alluminium, both of 99.999% purity, were melted together in graphite crusibles in a vacuum induction unit to give an approximate composition of 78 wt % Zn and 22 wt % Aluminium. The final analysis of the alloy is given in the Table II.

The alloy was cast into water cooled copper molds of 1.25 in. internal diameter. The ingots were hot rolled at 320°C to 7/8 in. square rods. Mechanical test samples were machined out of the rolled products to the specific dimensions. Subsequently the samples were heat treated.

6.2 SAMPLE SHAPE AND SIZE

Double shear specimens of the shape shown in Figure 19 were used for all mechanical tests. This kind of specimen shape gives two advantages, (i) the nature of stress developed in such a sample is pure shear, (ii) the stress remains constant over the cross-section bearing the load since the area of the sample does not change during the test deformation.

This kind of specimens were successfully by Dorn and his coworkers and have been recommended for constant stress creep tests.

6.3 HEAT-TREATMENT OF THE MATERIAL

The samples, after machining to the required dimensions, were given three heat-treatments:

(i) Homogenization

(ii) Quenching

and (iii) Annealing.

The samples were first given the homogenization treatment for 20 hours at 375°C. This was done with the purpose of levelling any compositional and structural inhomogeneities that may be introduced due to prior treatment. Heating for homogenization was carried out under argon atmosphere in a tube furnace with a Honeywell temperature controller. Precaution was taken to measure the actual temperature of the sample by providing a standardized chromet-alumel thermocouple very near the sample. The samples were suspended in the furnace by molybdenum wires.

Homogenization was followed by quenching the specimen from 375°C into an ice-water bath at 0°C.

The quenched samples were then given an annealing treatment to obtain various grain sizes. Annealing consisted of heating the quenched specimen slowly to 265°C (just below the eutectoid temperature) and holding it at that temperature for a specific time. Five different grain sizes were obtained by annealing for 5 different times, viz., 6 hours, 2 days, 2 weeks, 4 weeks and 5 weeks. Same furnace, as was used for homogenization, was utilized for annealing treatment.

6.4 MECHANICAL TESTS PROCEDURES

Two types of tests were performed to cover a wide range of strain rates, viz.,

(i) Constant-stress creep test in a creep set-up

and (ii) Instantaneous pulling-speed-change test in an Instron m/c creep test.

Specimens were crept at 250°C ($\pm$1°C) under constant stress. For heating the specimen silicone-oil bath, heated by an electric immersion heater, was used. The temperature was controlled by a Honeywell controller and continuously recorded. The oil bath was agitated to achieve temperature uniformity in the bath by bubbling argon gas through it. Additional thermocouples were fixed to the sides of the

samples so as to obtain accurate record of the sample temperature. The temperature fluctuations were within $\pm 1^{\circ}C$.

Shear displacement in the sample was continously recorded by using linear variable differential transformer. Creep curves were obtained to plotting displacement *versus* time curves. The straining, at a given stress, was continued until steady state was obtained over a considerable time span. The stress was then changed to a higher value and the test continued to a new steady state level. The procedure was repeated for 6 to 7 stress values, on the same sample, thus obtaining data over a wide range of stresses for a given grain size and temperature. Results were checked by another sample of the same grain size again. Creep curve for each stress level was plotted and steady state strain rates were determined graphically from these plots.

For the determination of activation energies, changes in temperature at constant stress, were carried out and corresponding steady state strain rates were determined.

6.5 INSTANTANEOUS PULLING-SPEED-CHANGE TESTS

These tests were carried out in the same way as suggested by Backofen *et al*. The procedure involved making sudden changes in pulling speed on an Instron

machine. Figure 20 gives a schematic diagram of the load time record covering a change of cross-head speed at time t* from V to V'. Transient hardening was eliminated from load comparisons by straining an additional 2 to 3% at the second speed, continuing to time 'A' in Figure 8. The extrapolation of the lower curve in the Figure was carried out beyond A to B to establish common strain for both speeds. Data for loads at various strain rates was recorded from cross-head speed of 2×10^{-4} in. per min. to 2 in. per minute.

6.6 CREEP SYSTEM

The creep system consisted, essentially, of three parts:

1. Heating
2. Sample fixture and loading
3. Measuring and Recording

6.6.1 Heating

Silicone oil which could be heated safely to 350°C was used for heating the samples. The oil was heated by the immersion heater of 1KWh capacity. It took approximately 2 hours to bring the sample to a temperature of 250°C. The oil bath was agitated with the help of argon gas bubbling

continuously. Oil bath prevented any oxidation of the sample.

6.6.2 Sample Fixtures and Loading

Split grips, as shown in Figure 22, were used. These were made of stainless steel. They were held in a cage (Figure 21); the central piece holding the central portion of the sample. The cage with the grips was attached to a rigid tall frame (Figure 21).

The sample was loaded through a wire rope suspended over two pulleys (Figure 21). The wire rope was hooked with the rod which was directly screwed into centre grip holding the specimen. Standard weights, for loading, were suspended at the loose end of the wire rope.

6.6.3 Measuring and Recording of Strain

The strain in the sample was measured by using a LVDT (Linear Variable Differential Transformer) (Figure 23) which measures the relative deflection of a magnetic core fitted to the middle tie rod.

Briefly, a LVDT is a linear motion, electromechanical transducer which produces an electrical output proportional to the displacement of a movable core. The transformer consists of a primary winding and two secondary windings

on a specially constructed bobbin. The core is a cylinder of ferromagnetic material which is free to move axially within the bore of the bobbin. When the core is at the neutral position of the transformer, the two secondary coils develop a very low combined output or null voltage. Movement of the core in either direction, then, produces an increasing voltage proportional to the distance moved.

LVDT Specifications:

Sensitivity	:	1.8 mV/volt-mil
Linear Range	:	$\pm$ 0.1"
Linearity	:	$\pm$ 0.1%
Tolerance	:	$\pm$ 0.00001 m.

The LVDT was assembled as shown in the Figure . The ac output of the LVDT was conditioned into dc signal. The dc output was then fed to a chart recorder.

6.6.3a Calibration of LVDT

The calibration of the LVDT was accomplished by means of the micrometer assembly. To calibrate the output in terms of the distance traversed by the core, the transformer was fixed and the core was moved. The displacement of the core was measured by the micrometer which was accurate to 0.00001". This calibration was done for each creep run.

6.7 INSTRON MACHINE TEST SET-UP

The specimen assembly was done in the same grips as were used in the creep tests. The central grip was attached to the fixed cross-head of the Instron and the cage assembly was fastened to the moving cross-head.

6.8 METALLOGRAPHY

Carbon replica technique was used to measure the grain size of the alloy after annealing and to record structural changes in the various ranges of strain rates. The details of the technique used are as follows.

Samples were polished by emery paper upto 4/0 grade and subsequently on diamond paste of 1 micron grain size. The samples were etched by Keller's reagent.

The plastic replicating paper was treated with methyl acetate and placed on the etched face of the sample taking care to prevent trapping of any air bubbles. On drying off of the methyl acetate, the replicating paper was stripped off the specimen. The above operation was repeated 3-4 times before a clean impression could be obtained on the replicating paper. The plastic replica was shadowed at a very narrow angle ($\lesssim 40°$) by evaporating carbon in a vacuum evaporating unit. The plastic base was

dissolved in methyl acetate by wetting the shadowed film in methyl acetate for about 24 hours. The slow dissolution of plastic was necessary to avoid curling of the carbon replicas.

Grain size was determined from electron micrographs of the surface replicas, using the method of mean linear intercept ($\bar{d}$) and converting to average spatial grain diameter (d) using the relationship[69] $d = 1.75\ \bar{d}$.

Table - II

Zn	-	77.45%
Al	-	22.5%
Impurities	-	0.05%

CHAPTER - 7

EXPERIMENTAL RESULTS

7.1 MICROSTRUCTURE

As-cast structure of the eutectoid alloy consisted of a typical lamellar structure of an eutectoid, with coarse elongated grains of second phase dispersed in the matrix in alternate layer from (Figure 24). The dark etching phase is Zinc rich solid solution (β) and the light etching phase Aluminium rich solid solution (α).

On quenching from single phase region, an extremely fine grained structure was obtained (Figure 25) with a grain size <0.5 m. Annealing at 265°C coarsened the structure and various grain sizes were obtained by annealing for different times.

7.2 GRAIN SIZE

Following grain sizes were obtained by annealing at 265°C.

Table III

Annealing Time	Average Grain Diameter (microns	Figure
6 hours	1.8 ± 0.1	25a
2 days	2.5 ± 0.1	25b

Contd.

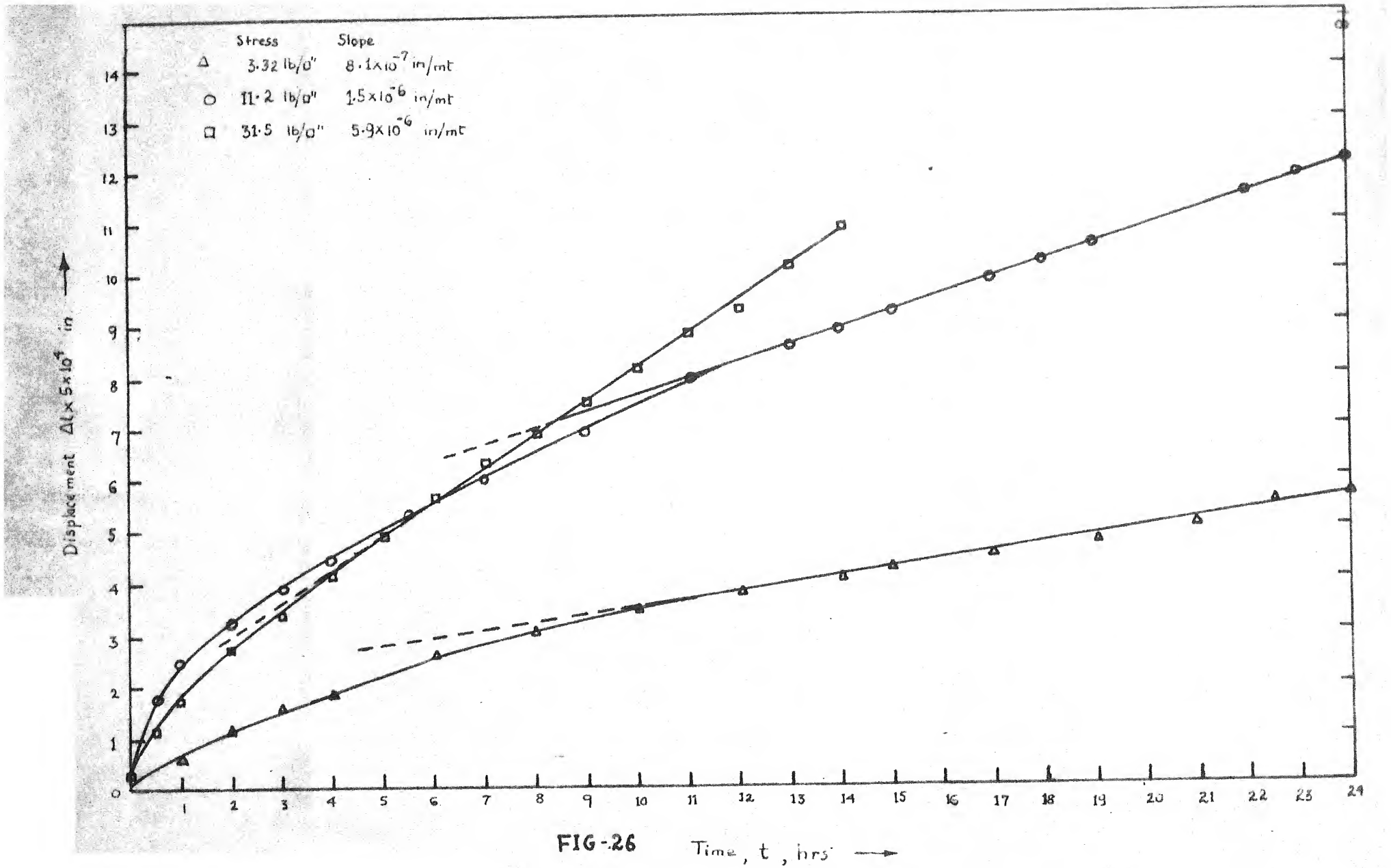
Stress
Slope
△ 3.32 lb/□" 8·1×10⁻⁷ in/mt
○ 11·2 lb/□" 1·5×10⁻⁶ in/mt
□ 31·5 lb/□" 5·9×10⁻⁶ in/mt
Displacement Δl × 5×10⁻⁴ in →
Time, t, hrs →

FIG-26

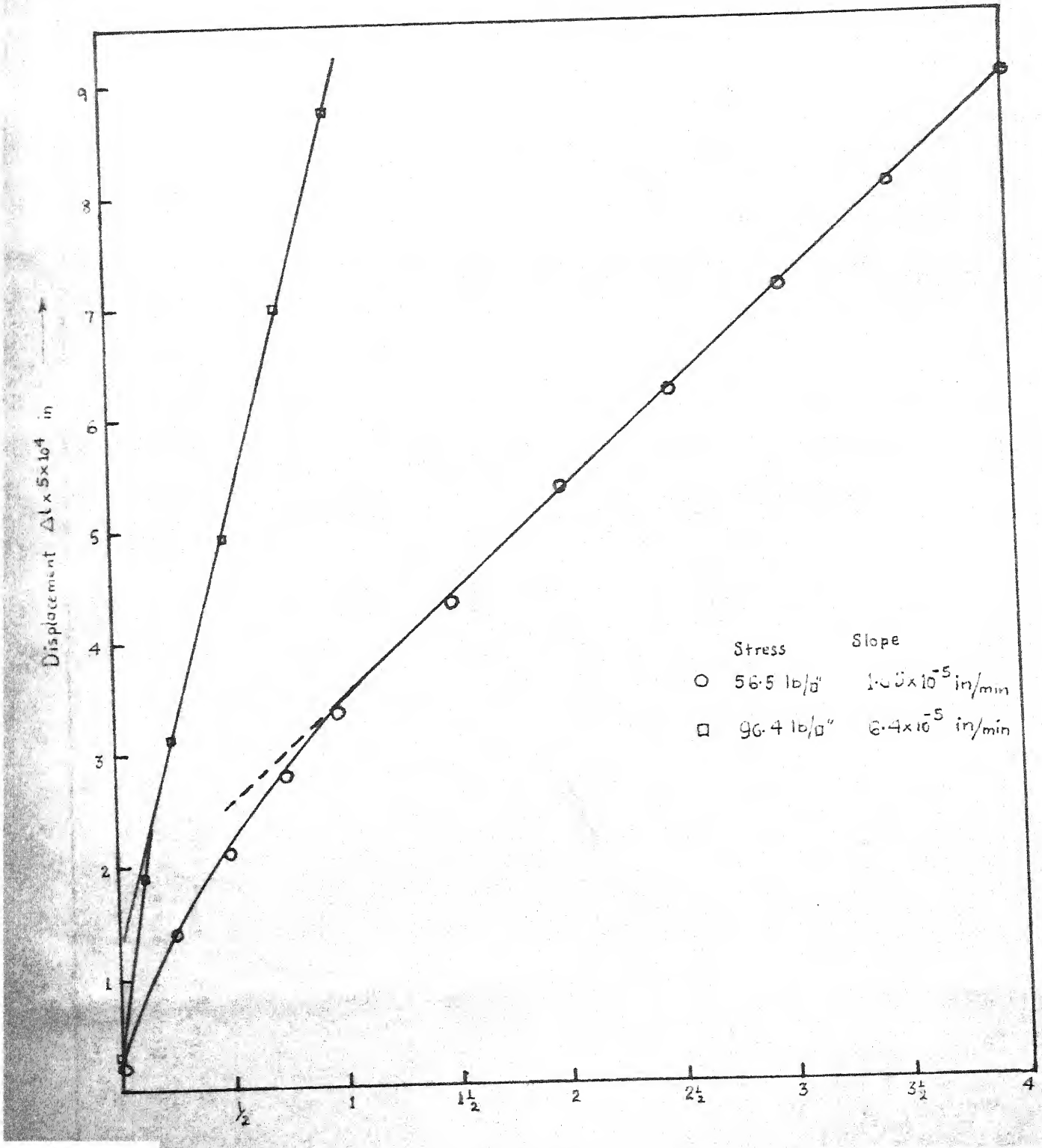
Displacement Δl x 5x10⁴ in
Time, t, hrs
Stress
Slope
○ 56·5 lb/□"
1·00x10⁻⁵ in/min
□ 96·4 lb/□"
6·4x10⁻⁵ in/min

FIG - 27

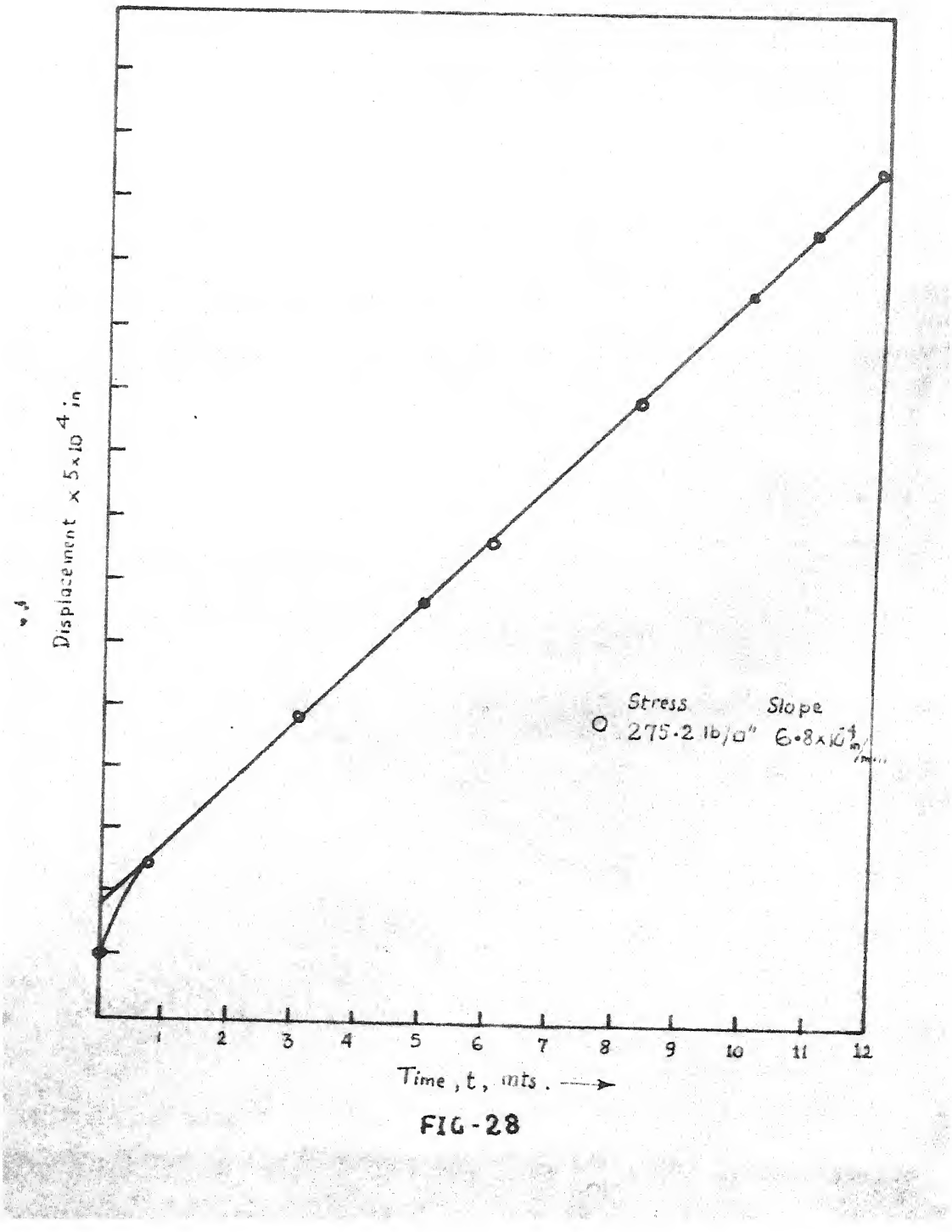
Displacement × 5×10⁻⁴ in.
Stress
Slope
○ 275·2 lb/□"
1
2
3
4
5
6
7
8
9
10
11
12
Time, t, mts. ⟶

FIG-28

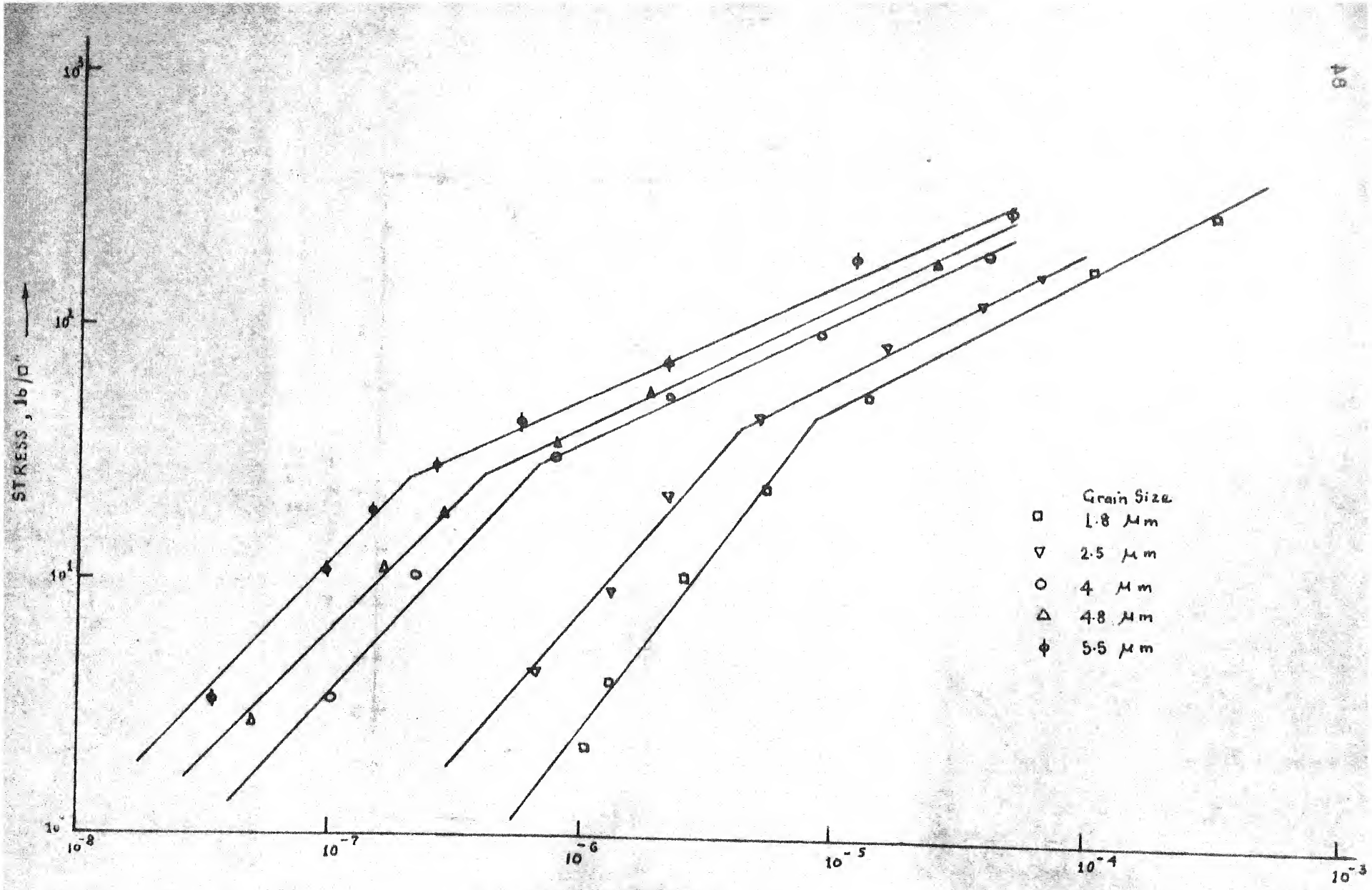
STRESS, lb/□"
10^3
10^2
10^1
10^0
10^{-8}
10^{-7}
10^{-6}
10^{-5}
10^{-4}
10^{-3}
STRAIN RATE, per second
Grain Size
1·8 μm
2·5 μm
4 μm
4·8 μm
5·5 μm

FIG-29

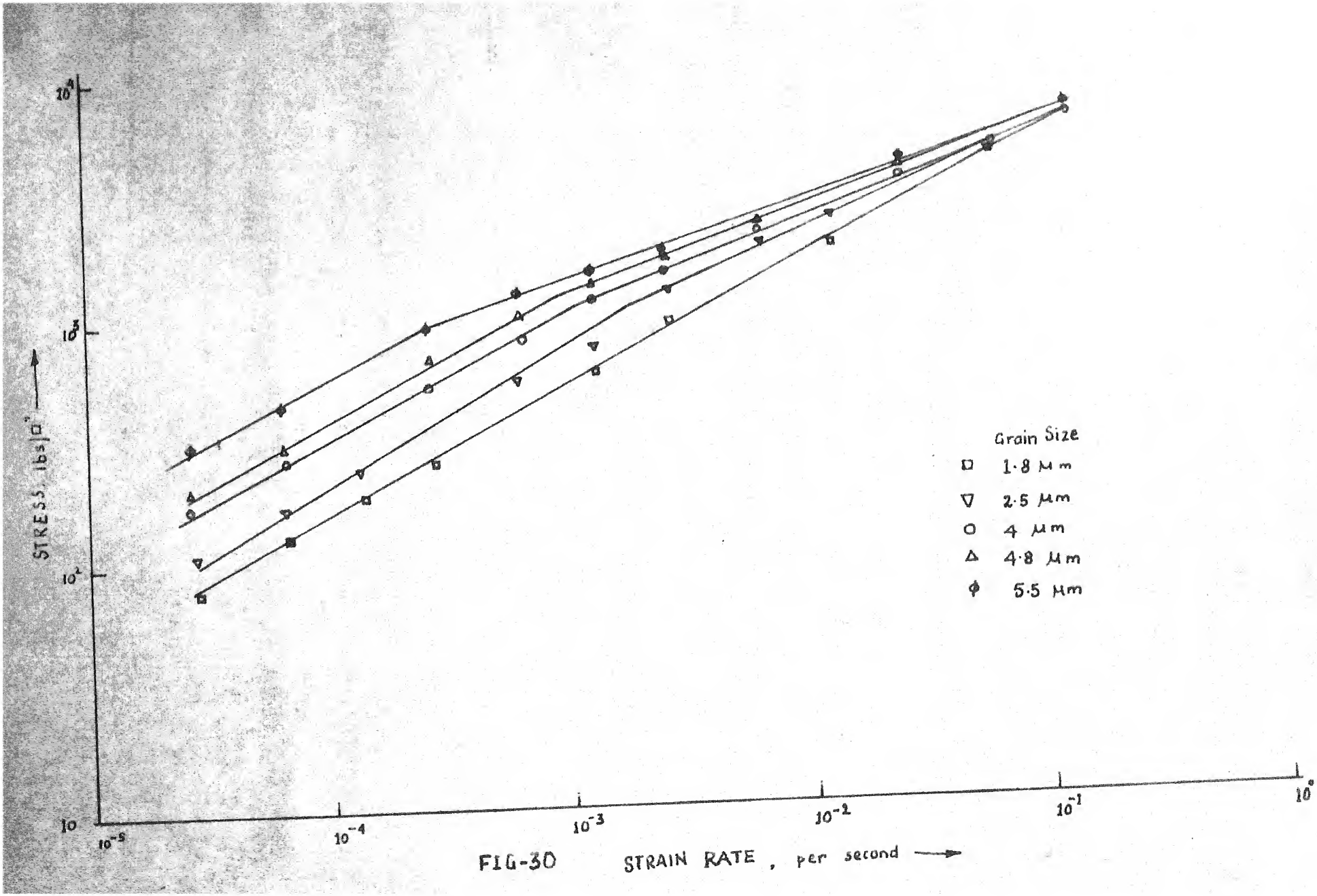
STRESS, lbs/□"
10^4
10^3
10^2
10
10^{-5}
10^{-4}
10^{-3}
10^{-2}
10^{-1}
10^0
STRAIN RATE , per second
Grain Size
□ 1·8 μm
▽ 2·5 μm
○ 4 μm
△ 4·8 μm
◇ 5·5 μm

FIG-30

Table III (Contd.)

Annealing Time	Average Grain diameter (microns)	Figure
2 weeks	4 $\pm$ 0.2	25c
4 weeks	4.8 $\pm$ 0.2	25d
5 weeks	5.5 $\pm$ 0.3	25e

7.3 CREEP CURVES

In Figures 26 to 28 are given the creep curves for a grain size of 4μ m. There is slight primary region indicated at certain stresses. Steady state followed the initial transient region. The data for other grain sizes are similar in nature (See Appendix IV). Steady state shear strain-rate ($\dot{\gamma}$) was measured graphically.

7.4 STEADY STATE SHEAR STRAIN RATE ($\dot{\gamma}$) vs. SHEAR STRESS (τ) CURVES

7.4.1 From Creep Test Data

Two distinct regions are marked on log $\dot{\gamma}$ vs. log τ curves (Figure 29): (i) Region I with an approximate slope of 1, and (ii) Region II with a slope 2. The slopes are independent of grain size. The effect of grain size is merely to shift the stress level at which the transition

from region I to II occurs. With decreasing grain size the stress at which the slope changes from region I to II shifts to a higher value. In other words, the extent of region I is increased.

7.4.2 From Instron Test Data

In this case, also, two distinct regions are marked on $\log \dot{\gamma}$ vs. $\log \tau$ curves (Figure 30) obtained from the Instron tests. The slope of the region at lower strain rates is approximately 2 and it changes to ~3.5 at higher strain rates.

7.4.3 Combined Plot of Creep and Instron Tests Data

The region II strain rates obtained in the creep tests and the results of the Instron tests at lower strain rates overlap, thereby establishing the validity of combining creep test data and that obtained on Instron.

The combined $\log \frac{\dot{\gamma} kT}{D_{gb} Gb}$ vs. $\log (\tau/G)$ plots (Figure 31) show three distinct regions I, II and III with slopes approximately 1 (region I), 2 (region II) and 3.5 (region III) respectively. These plots also show the variation of these regions with grain size. The slopes are independent of grain size.

(See values of k, Dg, G and b used in the calculations in Appendix V.)

OP

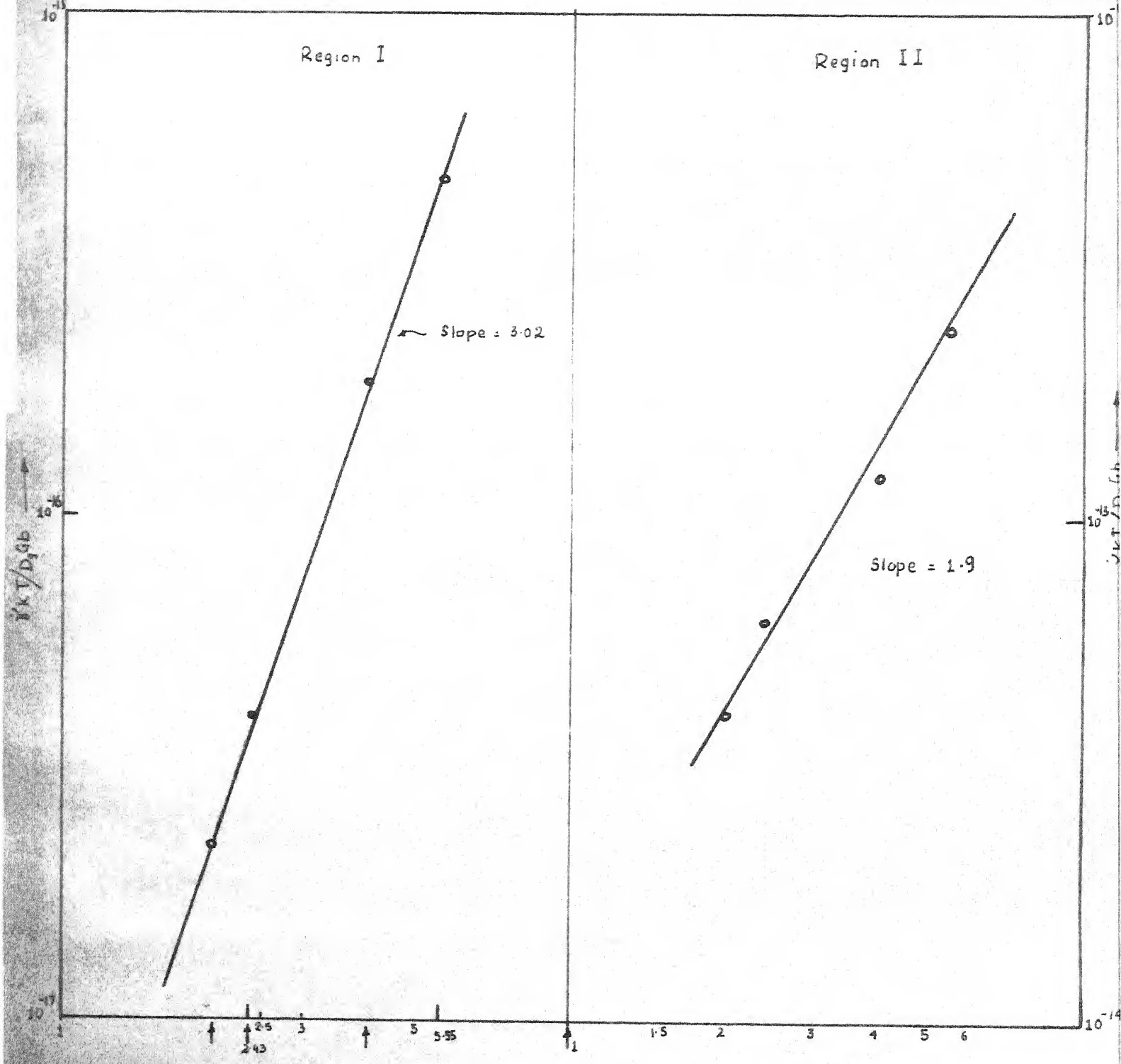

FIG-33

$\left(\frac{1}{d}\right)$x microns^{-1}

FIG-34

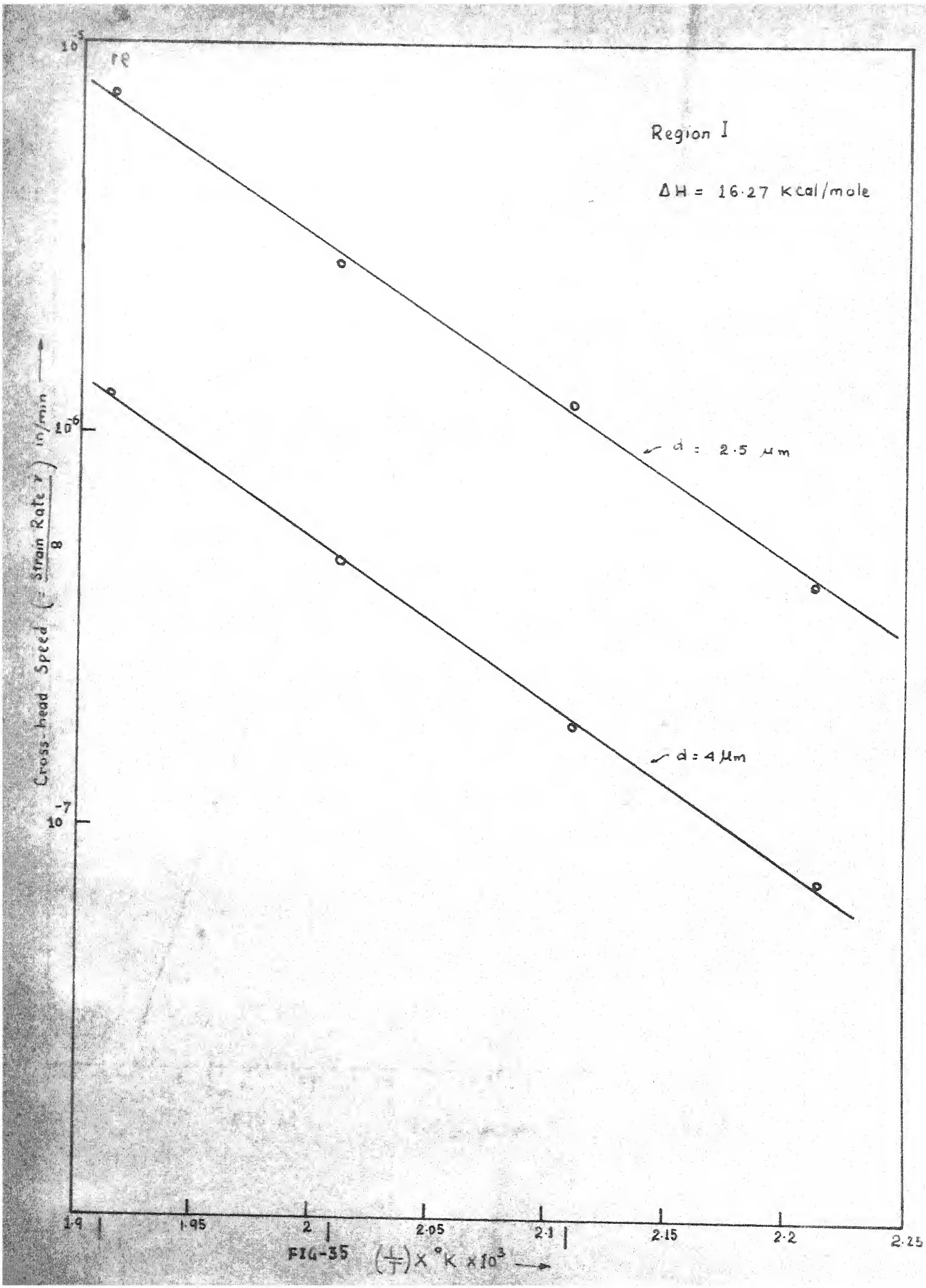
Fe
Region I
ΔH = 16·27 Kcal/mole
d = 2·5 μm
d = 4 μm
Cross-head Speed (= Strain Rate γ / 8) in/min
10⁻⁵
10⁻⁶
10⁻⁷
1·9
1·95
2
2·05
2·1
2·15
2·2
2·25
(1/T) X °K x 10³

FIG-35

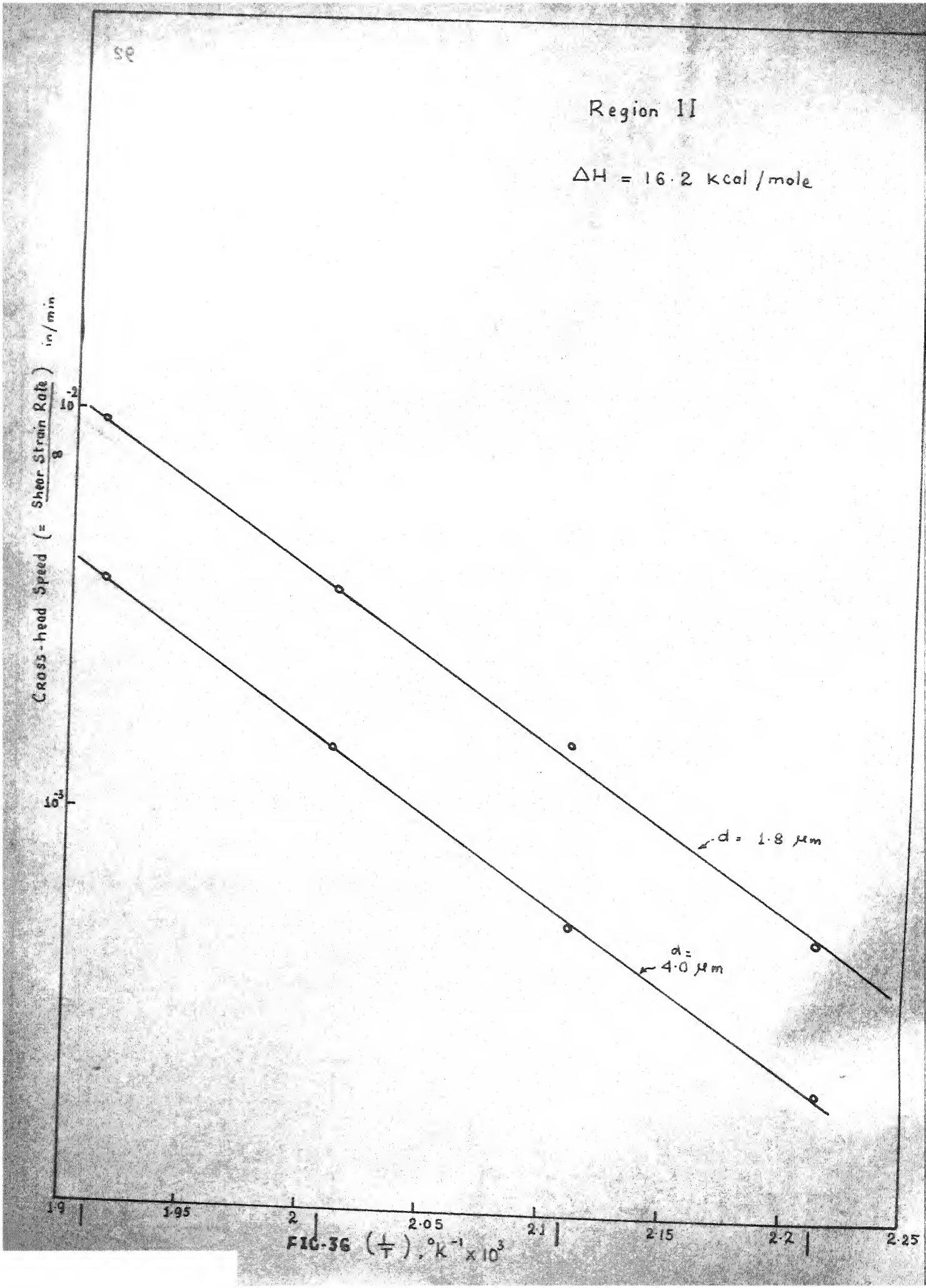
Region II
ΔH = 16·2 kcal / mole
Cross-head Speed (= Shear Strain Rate / 8) in/min
10^-2
10^-3
d = 1·8 μm
d = 4·0 μm
1·9
1·95
2
2·05
2·1
2·15
2·2
2·25
(1/T), °K^-1 x 10^3

FIG-36

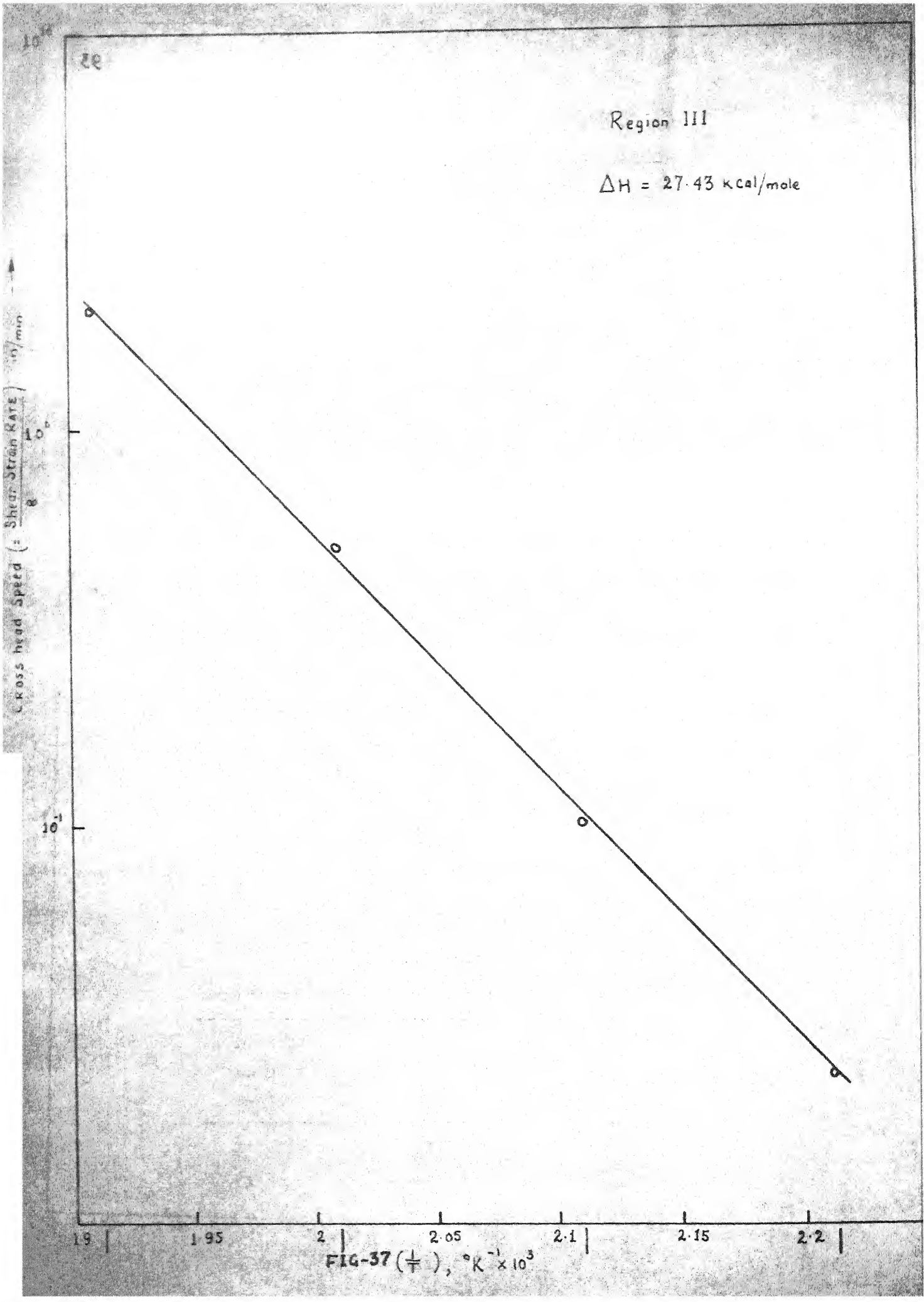
Region III
ΔH = 27·43 Kcal/mole
Cross head Speed (= Shear Strain RATE) in/min
10⁰
10⁻¹
1·9
1·95
2
2·05
2·1
2·15
2·2
FIG-37 (1/T), °K⁻¹ × 10³

7.5 VARIATION OF 'm' WITH STRAIN RATE (INSTRON DATA)

Figure 32 shows variation of strain rate sensitivity index 'm' with strain rate in case of 4 m grain size material. There is a region of 0.5 spread over ~$2\frac{1}{2}$ orders of magnitude. Similar plots were obtained for various other grain sizes.

7.6 SHEAR STRAIN RATE ($\dot{\gamma}$) —. GRAIN SIZE (d) AT CONSTANT STRESS (τ)

Figures 33 and 34 show approximately linear relationship between $\log \frac{\dot{\gamma} kT}{D_0 G b}$ and $\log \left(\frac{1}{d}\right)$ in region I and II. The slopes are ~3 and ~2 respectively. These plots have been obtained from Figures .

7.7 SHEAR STRAIN RATE ($\dot{\gamma}$) AND TEMPERATURE (T) AT CONSTANT STRESS (τ)

Approximately linear relationship is observed in all the three regions (Figures 35 to 37). The slopes are independent of grain size. The slopes in region I and II are nearly same whereas the slope in the region III is steeper. The activation energies derived from the present results are given in Table IV.

Table - IV

Region	Activation Energy
I	16.2 KCal/mol
II	16.27 KCal/mol
III	27.43 KCal/mol

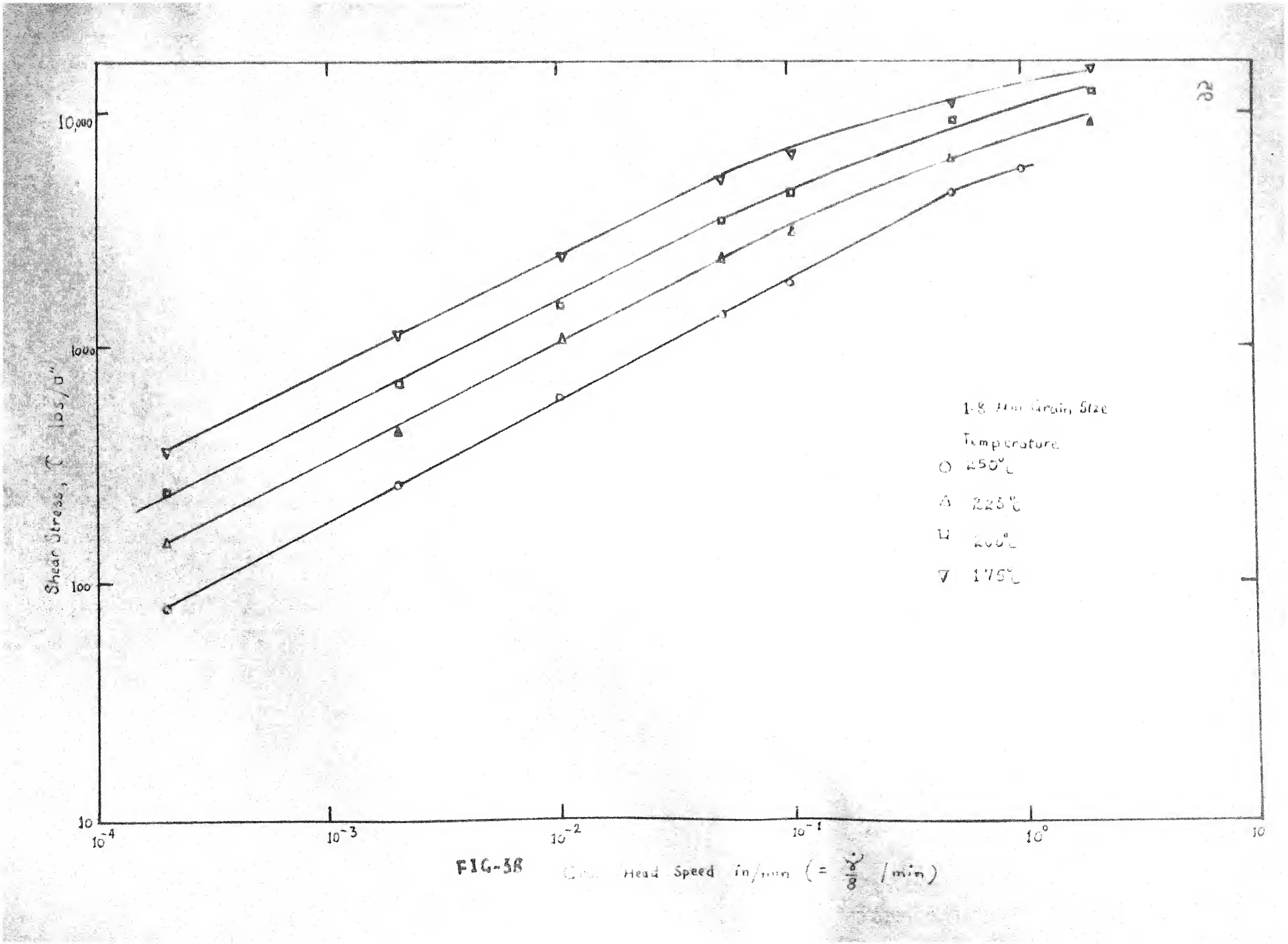

FIG-5B Cross Head Speed in/min (= $\frac{\dot{\delta}}{\delta}$ /min)

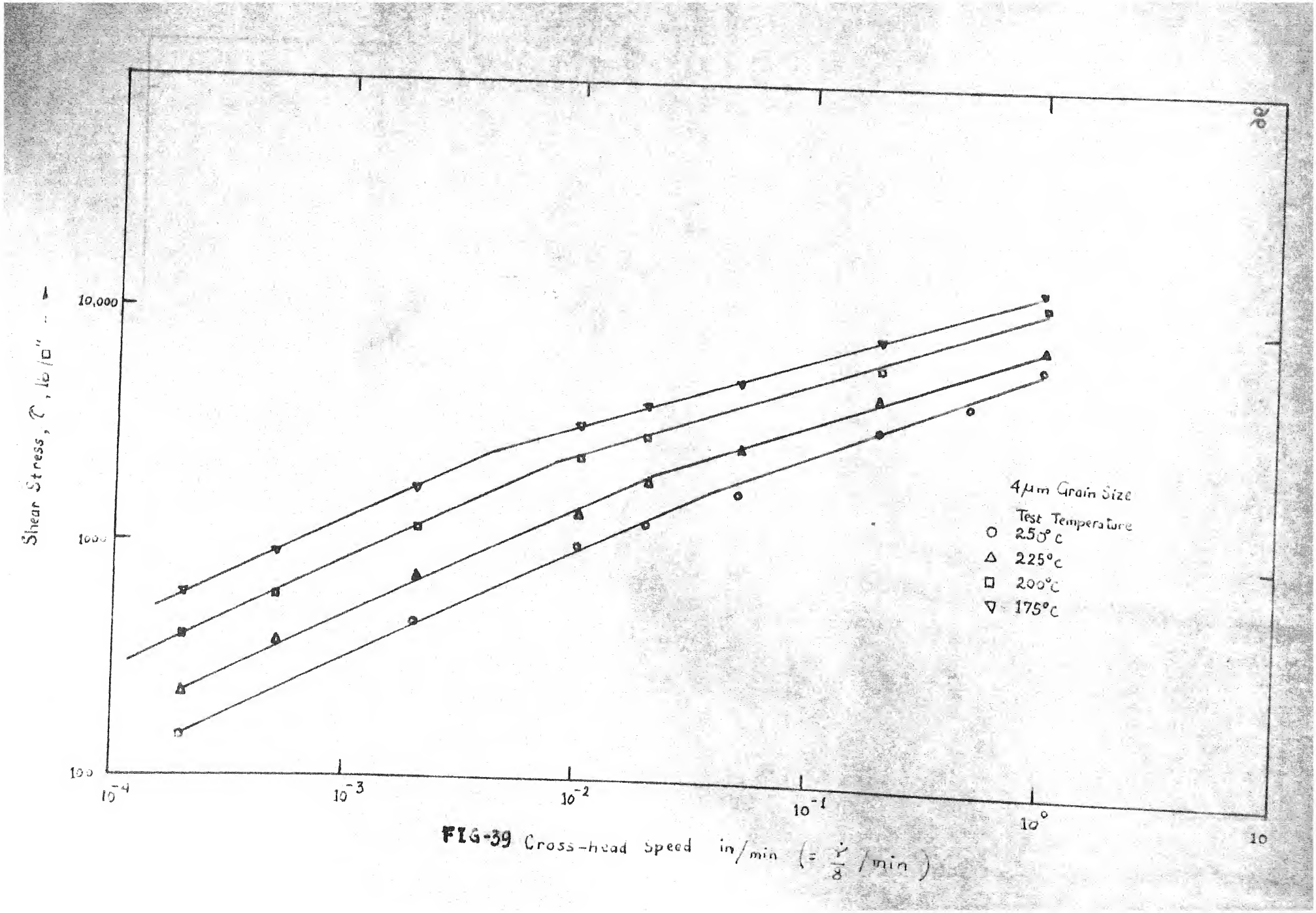

FIG-39 Cross-head Speed in/min $\left(= \frac{\dot{\gamma}}{8} \text{ /min}\right)$

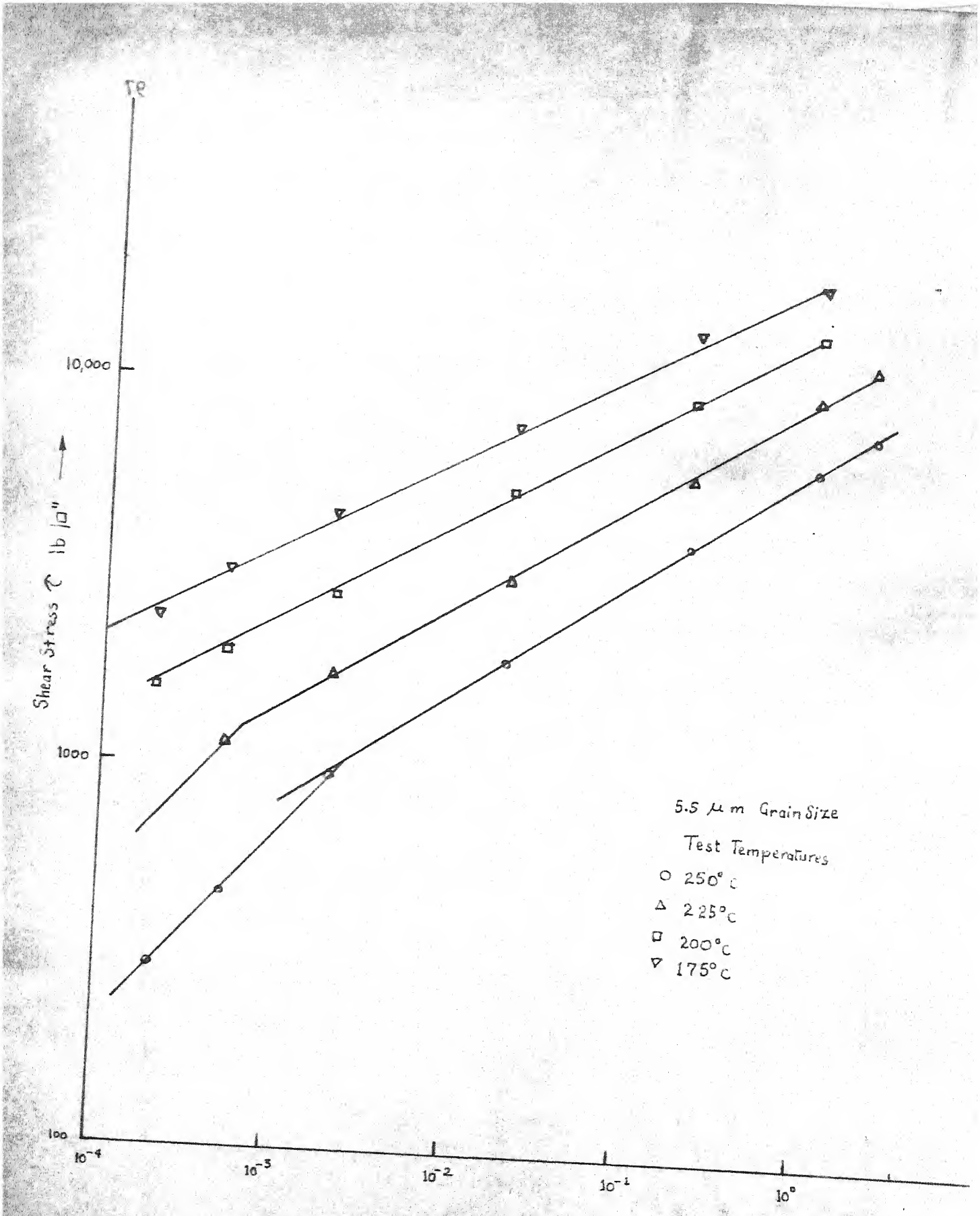
τR
10,000
1000
100
Shear Stress τ lb/□"
5.5 μm Grain Size
Test Temperatures
○ 250°C
△ 225°C
□ 200°C
▽ 175°C
10⁻⁴
10⁻³
10⁻²
10⁻¹
10⁰
Cross-head Speed in/min (= γ̇/8 per min) →

FIG-40

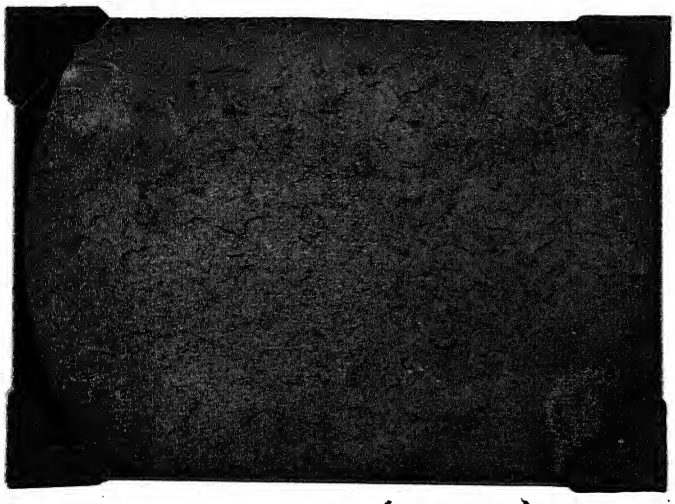

FIG-41 (X5000)

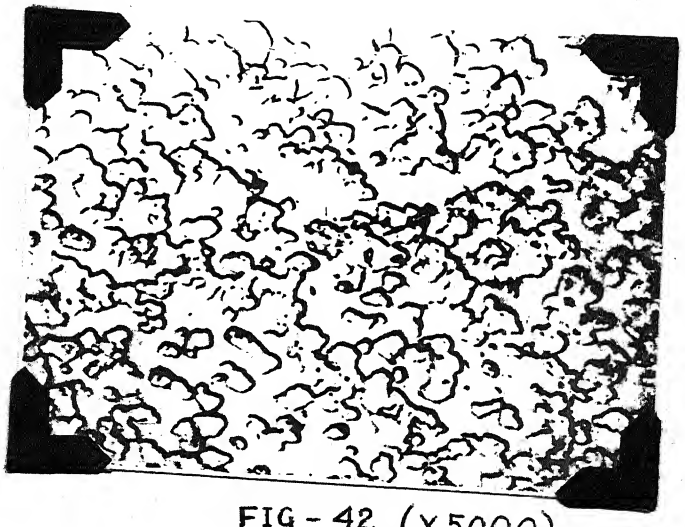

FIG-42 (X5000)

The plots, log $\dot{\varepsilon}$ vs. $\frac{1}{T}$, in regions II and III, are the cross plots from log σ vs. log $\dot{\varepsilon}$ plots obtained separately (Figures 38 to 40) for various temperature and for various grain sizes.

7.8 MICROSTRUCTURE AFTER DEFORMATION

There was very little grain growth during the prolonged creep testing. The microstructure after deformation in region I, II and III are shown in Figures (41 to 43). There is little difference in the annealed structure and the deformation structure, in region I. Whereas in region II, the structure appears slightly bulbus indicating rounding of sharp edges of the grains.

The structure after deformation in region III shows distinctly elongated grains indicating transgranular deformation.

7.9 SUMMARY OF THE MAIN RESULTS

The important results are summarised in Table V.

Table - V

Region	Activation Energy	Grain size dependence of strain rate	Stress dependence of strain rate
I	16.2 KCal/mole	$(\frac{1}{d})^3$	1
II	16.27 KCal/mole	$(\frac{1}{d})^2$	2
III	27.43 KCal/mole	$\sim(\frac{1}{d})^0$	~ 3.5

CHAPTER - 8

DISCUSSION

Three distinctive regions marked on the log $(\frac{\dot{\gamma} kT}{D_{gb}Gb})$ log (τ/G) curve indicate clearly that there are three distinct mechanisms controlling the deformation behaviour in Zn-Al eutectoid - each operative over a certain strain rate range. The possible mechanisms are discussed below.

8.1 MECHANISM OF DEFORMATION IN REGION I

The linearity of log $\dot{\gamma}$ vs. log τ and the slope of unity indicate a relationship of $\dot{\gamma} \propto (\tau)$. And the slope of 3 of the log $\frac{\dot{\gamma} kT}{D_{gb}Gb}$ vs $(\frac{1}{d})$ graph indicate a relationship of $\dot{\gamma} \propto (\frac{1}{d})^3$. Also, the activation energy obtained from the ln $\dot{\gamma}$ vs. $\frac{1}{T}$ graph, viz., 16.27 KCal/mole compares well with the activation energy for grain boundary diffusion in Zn (~14 KCal/mole)[70] which is the principal component of the alloy. Thus, a relationship of the following nature describes the deformation behaviour in the region I.

$$\dot{\gamma} = A (\tau)^1 (\frac{1}{d})^3 \exp (\frac{-\Delta H_{gb}}{kT})$$

where A = constant, ΔH_{gb} = Activation Energy for Boundary

diffusion. Reformulating it in a suitable form for a given temperature

$$\frac{\dot{\varepsilon} kT}{D_{gb} Gb} = A' \left(\frac{\tau}{G}\right)^1 \left(\frac{b}{d}\right)^3$$

where A' is a new constant, D_{gb} grain boundary diffusivity: $\left\{ D_o \exp \left(\frac{-\Delta H_{gb}}{kT}\right) \right\}$.

The reformulated equation compared very well with that for Coble mechanism of creep as reformulated by Dorn[7] et al. (Ref. 7).

$$\frac{\dot{\varepsilon} kT}{D_{gb} Gb} = A'_n \left(\frac{b}{d}\right)^3 \left(\frac{\sigma}{G}\right)^1$$

where A'_n, a constant has a value of ~ 48.

The Figure (31) gives the comparison between the experimental results and theoretical predictions of Coble mechanism. There is a very good agreement between them, indicating that grain boundary diffusion controlled mass transfer operates in the region I. It, thus, experimentally confirms the previous analysis of superplasticity data by Dorn et al. They had contended that, at low stresses, diffusional flow of matter, either through grain boundaries or through grains should make the principal contribution to the strain rate. Since grain boundary diffusion rates

are higher than the volume diffusion rates, such high strain rates, as are experimentally found in the Zn-Al system, could be explained only on the mechanism based on grain boundary diffusion. The confirmation of the mechanism comes in terms of activation energy value which is close to that for grain boundary diffusion.

There is an apparent conflict between the present results on Zn-Al eutectoid system and those on other superplastic systems, e.g., Pb-Sn (Ref. 71), Mg-Zk alloy (Ref. 72), in the strain rate region indicated by region I. In the latter case the slope of the $\log \dot{\gamma}$ vs. $\log \tau$ approximates 4 to 5 instead of one as in the present observations. The increase in slope is attributed to a possible back stress. If it is true that such a back stress is really operating and obstructing the diffusional flow then its value must be extremely low in the Zinc-Aluminium system. As a consequence its effect is not shown on the $\dot{\gamma}$ (τ) results.

The strain rate dependence of unity on stress at low stresses levels has been previously observed in other systems too (Ref. 26). These were also fine grained materials.

The concept of critical yield stress for creep may not hold good in the Zinc-Aluminium eutectoid system.

8.2 MECHANISM OF DEFORMATION IN REGION II

The slope of the log $\dot{\gamma}$ vs. log (τ) approaches two and the slope of log $\frac{\dot{\gamma} kT}{D_g Gb}$ vs. log $(\frac{1}{d})$ approaches 2. Moreover, the activation energy of 16.2 KCal/mol, determined experimentally, compares well with the activation energy for grain boundary diffusion in Zinc. Thus, the strain rate could be expressed by

$$\dot{\gamma} = K (\tau)^2 (\frac{1}{d})^2 \exp (\frac{-\Delta H_{gb}}{kT})$$

Reformulating the expression

$$\frac{\dot{\gamma} kT}{D_{gb} Gb} = K' (\frac{\tau}{G})^2 (\frac{b}{d})^2$$

This expression compares well with that derived by Ball and Hutchison and that by Mukherjee[62]. Their models are based on the grain boundary sliding mode of deformation. The metallographic evidence confirms the previous observation - slight rounding off of the grains. The previous evidence of large GBS associated with m = 0.5 (i.e. 2 for 1/m in the reformulated expression) and the present results confirming the activation energy to be that for grain boundary diffusion makes a strong case for GBS as the

operative mechanism in the region II.

Though the details of the Ball-Hutchison model are not very clear, the basic fact remains that the grain boundary sliding controls the deformation over an extensive range of strain rates. Unlike the suggestion by Alden and Hart, it is not a mere transition but a region spread over 4 orders of magnitude. The present results are in conformity with those of Ball-Hutchison over similar strain rates. The value of the constant K' in the present case works out to be 1.5×10^3 which compares favourably with 1×10^3 given by Ball-Hutchison data (calculated for shear stress and shear strain rate relationship).

8.3 MECHANISM OPERATING IN REGION III

As the stress is increased from region II to region III, the deformation, predominantly by GBS gives way to deformation by slip. The deformation is chiefly confined to the grains. The strain rate tends to be independent of grain size. The activation energy of 27.43 KCal/mole indicate volume diffusion controlled mechanism. The stress dependence of the strain rate is nearly 3.5 which is similar to that given by the glide controlled mechanism. The expression for the rate would be

$$\frac{\dot{\gamma} kT}{D_v Gb} = A'' \left(\frac{\tau}{G}\right)^{3.5}$$

Microstructural changes are consistent with the proposed mechanisms in various regions. In region I, pure diffusional flow, devoid of any significant dislocation activity causes no significant change in the annealed condition. In region II, since there is some accommodation needed in terms of dislocation motion near the grain boundaries there is rounding (bulbus) of the Zinc rich phases. In region III, transgranular deformation involving slip causes grain elongation.

CONCLUSIONS AND RECOMMENDATIONS

Following conclusions are drawn from the present investigation:

1. There are three distinct mechanism controlling the deformation of Zn-Al eutectoid between 10^{-8} to 1 per second strain rate range.

2. At very low strain rates (and stresses) the deformation is controlled by stress directed vacancy migration along grain boundaries, i.e., Coble mechanism. This has been clearly borne out, for the first time, both in terms of activation energy for deformation and grain size dependence.

3. Beyond the Coble-mechanism controlled region, there is an extensive region over which grain boundary sliding is the principal mode of deformation. It is grain boundary diffusion controlled. It is not a mere transition region between two modes of deformation.

4. The grain size dependence of strain rate was confirmed to be '2' in the region II which coincides with the so called superplastic strain rate range.

5. The deformation in the high strain rate range is nearly independent of the grain size and the mode of deformation is dislocation motion controlled creep through the grains.

RECOMMENDATIONS

The present investigation establishes a definite need to reexamine data on other superplastic systems to define the relation between diffusional creep, grain boundary sliding and the anomalous plastic behaviour, viz., superplasticity.

Controlled experiments at extremely small strain rates ($<10^{-9}$ per second) need to be done to explore the possibility of back stress in Zn-Al eutectoid system and determine the same. If there is back stress, as reported by others, its origin need to be investigated thoroughly. Proper understanding of the origin of back stress would be of tremendous consequence in controlling creep behaviour of materials.

REFERENCES

1. W. Rosennain, J.L. haughton and K.E. Bingham, J. Inst. Metals, 1920, 23, 261.

2. W.A. Backofen, I.R. Turner, and D.H. Avery, Trans. Amer. Soc. Metals, 1964, 57, 980.

3. D.L. Holt, Trans. Met. Soc. A.I.M.E., 1968, 242, 25.

4. T.H. Alden and H.W. Schadler, ibid., p.825

5. P. Chaudhari, Acta Met., 1967, 1771.

6. A. Ball and M.M. Hutchison, Met. Sci. J., 1969, 3, 1.

7. J.E. Bird, A.K. Mukherjee and J.E. Dorn, Report on the International Conference on Quantitative Relation Between Properties and Microstructure, Haifa, Israel, 1969.

8. J.J. Kanter, Trans. Met. Soc. A.I.M.E., 1938, 131, 385.

9. J.E. Dorn, J. Mech. Phys. Solids 1955, 3, 385.

10. W. Kauzmann, Trans. Met. Soc. A.I.M.E., 1941, 143, 57.

11. S. Dushman, L.W. Dunbar and H.H. Huthsteiner, J. Appl. Phys. 1944, 15, 108.

12. F. Garofalo, 'Fundamentals of Creep and Creep Rupture in Metals', Macmillan, N.Y., 1965.

13. O.D. Sherby, Acta Met. 1962, 10, 135.

14. J.E. Dorn, 'Creep and Recovery', A.S.M., Cleveland, 1957.

15. O.D. Sherby, R.L. Orr and J.E. Dorn, Trans. Met. Soc. A.I.M.E., 1954, 200, 71.

16. H. Conrad, 'Mechanical Behaviour of Materials at Elevated Temperatures', McGraw Hill Book Co. Inc., N.Y., 1961, 149.

17. A.H. Cottrell and V. Aytekin, J. Inst. Metals, 1950, 77, 389

18. C. Rossard, Rev. Mét., 1966, 63 (3), 225.

19. E. Hart, Acta Met., 1967, 15, 351.

20. F.R.N. Nabarro, Report of a Conference on the Strength of Solids, p.75, The Physical Society, London (1948).

21. C. Herring, J. Appl. Phys., 1950, 21, 437.

22. R.L. Coble, 1963, J. Appl. Phys., 34, 1679.

23. A.L. Pranatis and G.M. Pound, Trans. Met. Soc. A.I.M.E., 1955, 203, 664.

24. A.P. Greenough, Phil. Mag., 1952, 43, 1075.

25. E.D. Hondros, Phys. Stat. Sol., 1967, 21, 375.

26. R.B. Jones, Nature, 1965, 207, 70.

27. I.M. Bernstein, Trans. Met. Soc. A.I.M.E., 1967, 239, 1518.

28. H. Tagai, and T. Zisner, J. Amer. Ceram. Soc., 1968, 59, 479.

29. I.M. Lifshitz, Soviet Physics JETP, 1963, 17, 909.

30. G.B. Gibbs, Mem. Sci. Rev. Met., 1965, 62, 775.

31. J.E. Harris, R.B. Jones, G.W. Green Wood and M.J. Ward, J. Aust. Inst. Metals, 1969, 14, 154.

32. G.B. Gibbs and J.E. Harris, C.E.G.B. Berkeley Nuclear Lab. Report No.RD/B/N/1327, 1969.

33. N.F. Mott, Surveys in Mechanics, Cambridge Univ. Press, N.Y., 1956, 32; Nature 1955, 175, 365.

34. J. Weertman, J. Appl. Phys., 1957, 28, 362.

35. J. Weertman, ibid., 1957, 28, 1185.

36. R.N. Stevens, Met. Rev., 1966, 11, 129.

37. R.C. Gifkins and K.U. Snowden, Nature, 1966, 212, 916.

38. R.C. Gifkins and K.U. Snowden, Trans. Met. Soc. A.I.M.E., 1967, 239, 910.

39. K.F. Hale, Y. Ishida, T.L. Lin and D. McLean, 1966, Sixth Intnl. Congress for Electron Microscopy, Kyoto, edited by R. Uyeda (Tokyo: Maruzen), 295.

40. T.L. Lin and D. McLean, Metal Sci. J. 1968, 2, 108.

41. Y. Ishida, M. Henderson Brown, Acta Met., 1967, 15, 857.

42. F.G. Langdon, Phil. Mag., 1970, 22, 689.

43. G.B. Gibbs, Mater. Sci. Eng., 1967-68, 2, 268.

44. A.H. Cottrell and V. Aytekin, J. Inst. Met., 1950, 77, 389

45. N.F. Mott, Phil. Mag., 1953, 44, 742.

46. 'Metals Hand Book' (1948), American Soc. for Metals.

47. A.A. Bochvar and Z.A. Sviderskaya, Izvest. Akad. Nauk S.S.S.R., 1945, 9, 821.

48. A.A. Presnyakov and V.V. Chervyakova, Fizika Metallov i Metallovederic, 1959, 8, 114.

49. E.E. Underwood, J. Metals, 1962, 14, 914.

50. D. Oelschlagel, J. Japan Inst. Metals, 1966, 6, 11.

51. K. Nuttall and R.B. Nicholson, Phil. Mag., 1968, 17, 1087.

52. R.H. Johnson, C.M. Packer, L. Anderson and O.D. Sherby, ibid., 1968, 18, 1309.

53. E.C. Bingham, U.S. Bureau of Standards, Scientific Paper No.278.

54. D.H. Avery and W.A. Backofen, Trans. Amer. Soc. Metals, 1965, 58, 551.

55. D.L. Holt and W.A. Backofen, Trans. Amer. Soc. Metals, 1966, 59, 755.

56. R.B. Jones, Private communication.

57. W.A. Backofen, F.J. Azzarto, G.S. Murty and S.W. Zehr, 'Ductility', p.279, 1967, London (Chapman and Hall).

58. D.H. Avery and J.M. Stuart, 'Surfaces and Interfaces Vol. II", edited by Burke, Reed and Weiss, p.371, 1968.

59. A. Karim, 'Ultrafine-Grain Metals', edited by Burke and Weiss, p. 295, 1969.

60. R.B. Jones and R.H. Johnson, Trans. Amer. Soc Metals, 1966, 59, 356.

61. C.M. Packer and O.D. Sherby, Trans. Amer. Soc. 1967, 60, 21.

62. A.K. Mukherjee, Mat. Sc. & Engg., 1971, 8, 83.

63. T.H. Alden, Acta Met., 1967, 15, 469.

64. E.W. Hart, Acta Met., 15, (1967) 1545.

65. H.W. Hayden, R.C. Gibson, H.F. Merrick and J.H. Brophy, Trans. Amer. Soc. Metals, 1967, 60, 3.

66. C.M. Packer, Ph.D. Thesis, Stanford Univ., Calif., 1967.

67. R.H. Johnson, C.M. Packer, L. Anderson, and O.D. Sherby, Phil. Mag., 1968, 18, 1309.

68. K.D. Fike and H.J. Rack, Trans. Amer. Soc Metals, 1969, 62, 537.

69. J.H. Woodhead, Private communication.

70. E.S. Wajda, Acta Met., 1954, 2, 184.

71. D.L. Holt and W.A. Backofen, Trans. Amer. Soc. Metals, 1966, 59, 755.

72. A. Karim, 'Ultrafine-Grain Metals', edited by J.J. Burke and V. Weiss, p.295, 1970, Syracuse Univ. Press, New York.

APPENDIX - I

MATERIALS EXHIBITING STRUCTURAL SUPERPLASTICITY

Base Metal	Alloying Elements	Grain size	Temperature °C
Aluminium	33 Cu	1-2	440-530
	12.4 Cu	-	500
Cadmium	26 Zn	1-2	20
Chromium	40 Ru	-	1280
Cobalt	10 Al	0.4	1200
Copper	10 Mg	-	700
	10-12 Al	-	500
	10 Al : 4 Fe	-	500
	38-50 Zn	-	450-650
Iron	0.14 C : 1.2 Mn : 0.5 P 0.1 V	2	900
	0.34C : 0.47Mn : 2.0 Al	2	900
	0.42C : 1.9 Mn	1-2	730
	26 Cr : 6.5 Ni)	2	870-980
	30 Cr : 6.0 Ni)		
Lead	20 Sn	3	20
	5 Cd	4	0
Magnesium	0.5 Zr	20	500
	6 Zn : 0.6 Zr	0.5	270-310
	23 Ni	-	450
	30 Cu		450
	33 Al		400
Nickel	nil	8	820
	39 Cr : 8 Fe : 2 Ti	2	980
Tin	5 Bi	1	20
	2-38 Pb	1-2	20
	33 Cd	1-2	20

Table Contd...

Base Metal	Alloying Elements	Grain size	Temperature °C
Titanium	6 Al : 4 V	6	900-980
	5 Al : 2.5 Sn	18	1000
Zinc	nil	1-2	0-20
	0.5 Al	1-2	20
	5 Al	1-2	200-360
	22 Al	1-2	200-260
	40 Al	1-10	250
Zirconium	Ziryaloy-4	12	900

APPENDIX - II

PHENOMENOLOGICAL EXPLANATION OF SUPERPLASTIC BEHAVIOUR

It is necessary to examine briefly the mechanics of stable flow under tensile forces in order to introduce the parameter of strain rate sensitivity (SRS). The explanation follows that given by Backofen et al.

A ductile material when stretched by a tensile force can deform uniformly only while stable flow occurs (homogeneous deformation). The limit of the stable flow is marked by the onset of geometrical instability - sudden concentration of deformation at point - called necking.

Necking generally occurs in a material elongated under tensile load. Because $V = A.l$ is fixed during plastic deformation, an incremental extension, δl, may be offset by incremental area reduction, δA, to insure

$$\delta V = A\,\delta l + l\,\delta A = 0 \qquad \text{---(1)}$$

$$\text{or} \quad \frac{\delta l}{l} = -\frac{\delta A}{A} = \delta \varepsilon$$

which defines an increment of true strain ε. The area reduction can have two effects.

1. It causes a loss in load carrying ability of an amount $\sigma \delta A$, where σ is the prevailing tensile flow stress

when δA occurs

$$\text{Rate of loss} = \frac{\sigma \delta_A}{\delta A} = \sigma$$

2. It may also cause increased load carrying capacity if strain hardening occurs, i.e. $\frac{d\sigma}{d\varepsilon} > 0$

Now, to avoid microscopic necking, the incipient neck should not grow, so $\frac{d\sigma}{d\varepsilon} > \sigma$.

The usual 'exhaustion' of the strain hardening capacity in metals is responsible for a $\frac{d\sigma}{d\varepsilon}$ to fall as ε increases and necking would begin when $\frac{d\sigma}{d\varepsilon} = \sigma$.

In more general terms, σ is a function of many variables

$$\sigma = \sigma(\varepsilon, \dot{\varepsilon}, T, \gamma \ldots\ldots) \quad \text{---(2)}$$

where ε is strain, $\dot{\varepsilon}$ = strain rate, T = Absolute temperature of deformation and γ = surface energy

Differentiating

$$\frac{d\sigma}{d\varepsilon} = \frac{\partial \sigma}{\partial \varepsilon} + \left(\frac{\partial \sigma}{\partial \dot{\varepsilon}}\right)\left(\frac{d\dot{\varepsilon}}{d\varepsilon}\right) + \left(\frac{\partial \sigma}{\partial T}\right)\left(\frac{dT}{d\varepsilon}\right) + \left(\frac{\partial \sigma}{\partial \gamma}\right)\left(\frac{d\gamma}{d\varepsilon}\right) \quad \text{---(3)}$$

This means that strain induced hardening to counteract neck formation may have multiple origins; metallurgical cold work (i.e., strain hardening), and increase in strain rate, a drop in temperature, or a rise in surface energy. The one to predominate determines many details of normal material behaviour.

At temperatures above 0.5 Tm, as are the temperatures in superplastic phenomenon, contribution from $\frac{\partial \sigma}{\partial \varepsilon} \rightarrow 0$ and the second term in the equation (3) becomes more important; in other words the strain rate sensitivity $(\frac{\partial \sigma}{\partial \dot{\varepsilon}})$.

A convenient $\sigma(\dot{\varepsilon})$ relationship is $\sigma = K\dot{\varepsilon}^m$, in which m is a very useful index of strain rate sensitivity given by $m = d \log \quad / d \log \quad .$

Now, $\frac{P}{A} = \sigma = K\dot{\varepsilon}^m$ ——— (4)

where P = load, A = Area of cross-section.

At any point along a rod in tension

$$\dot{\varepsilon} = \frac{\delta l}{l} \frac{1}{t} = -\frac{1}{A} \frac{dA}{dt} \quad \text{——— (5)}$$

Combining (4) and (5) $-\frac{dA}{dt} = (\frac{P}{A})^{1/m} \left[\frac{1}{A^{\frac{1-m}{m}}} \right]$.

As long as m is < 1, the smaller the cross-section the more rapidly it is reduced. As m approaches 1, the reduction rate at all cross-sections approaches a common level. When m=1, the flow is Newtonian viscous and $\frac{dA}{dt}$ is independent of A, so that any cross-sectional irregularities are simply preserved during pulling.

In a superplastic metal, where m is high but < 1, this effect still exists. In a nonsuperplastic material in which m is always < 0.2, a pronounced change in cross-

section (neck) occurs where the area is a minimum and stress higher than elsewhere. Any local stress increase in the superplastic metal produces only small change in strain rate and consequently such regions tend to deform at a rate not significantly different from the rest of the specimen and a very much extended version of a neck results. This effect makes it appear almost as if the specimen was not necking at all.

APPENDIX - III

EXPERIMENTAL TECHNIQUES LEADING TO DETERMINATION OF THE OBSERVED ACTIVATION ENERGIES

Principally, there are three different types of tests which are usually employed to determine the activation energy for creep

1. Isothermal tests

Here the temperature and stress are held constant. From graphical determination, the value of $\dot{\varepsilon} = \frac{d\varepsilon}{dt}$ is obtained for constant value of the strain from ε vs. t plot. A method of treating the derived strain rate data arises from the consideration of the general rate equation

$$\dot{\varepsilon} = A' f(\sigma) \exp\left\{-\frac{\Delta H}{RT}\right\} \quad \text{for} \quad \varepsilon = \text{constant}$$

$$\text{or} \quad \ln \dot{\varepsilon} = \ln A' + \ln\left\{f(\sigma)\right\} - \frac{\Delta H}{RT}$$

Differentiating with respect to $\left(\frac{1}{T}\right)$ gives

$$\frac{\partial \ln}{\partial\left(\frac{1}{T}\right)} = -\frac{\Delta H}{R} \quad \text{for} \quad \begin{cases} \varepsilon = \text{constant} \\ \sigma = \text{constant} \end{cases}$$

Graphical solution involves the use of semilogarithmic plot of log against the reciprocal of the absolute

temperature for constant values of the applied stress and initial structure.

2. Incremental Loading Creep Tests

In these tests, the stress is increased, starting from zero, in small but sudden increments. Since the tests are performed at constant temperatures, the strain rates just before and immediately after each stress change are observed to evaluate the creep rate at the mean value of the applied stress. The activation energy is then evaluated from an appropriate cross-plot of strain rates and the reciprocal of the temperature at constant value of stress.

3. Change of Slope Method

These tests involve making an abrupt change in the test temperature during a constant stress or constant-load creep test. This technique is known as 'Differential temperature creep testing'. The abrupt changes in temperature cause appropriate changes in the creep rate. The substructure is assumed to be identical just preceding and immediately following such abrupt changes in temperature. Since the stress is effectively the same just before and immediately following the change in temperature, the change in creep rate must be exclusively attributed to the imposed temperature change. Assuming, a single activation process,

the creep rate $\dot{\varepsilon}_1$, and $\dot{\varepsilon}_2$ just preceding and immediately following an abrupt change in temperature T to $T_2 = T + \Delta T$ are related by

$$\dot{\varepsilon}_1 \exp\left\{\frac{\Delta H\ (T_1)}{RT_1}\right\} = \dot{\varepsilon}_2 \exp\left\{\frac{\Delta H\ (T_2)}{RT_2}\right\}$$

$$R \ln \frac{\dot{\varepsilon}_2}{\dot{\varepsilon}_1} = \frac{\Delta H\ (T_1)}{T_1} - \frac{\Delta H\ (T_2)}{T_2}$$

$$= \frac{d\ (\Delta H/T)}{d\ (1/T)}\ \Delta\left(\frac{1}{T}\right)$$

$$= \Delta H\left(\frac{1}{T_1} - \frac{1}{T_2}\right)$$

so that $$\Delta H = \frac{RT_1T_2}{\Delta T} \ln\left(\frac{\dot{\varepsilon}_2}{\dot{\varepsilon}_1}\right).$$

APPENDIX - IV

CREEP TEST AND INSTRON TEST DATA FOR GRAIN SIZES

1.8, 2.5, 4.8 and 5.5 MICRON GRAIN SIZES

Table - VI

Creep Test Data for 1.8 μm Grain Size

Temperature, °K	Shear Stress (τ) lb/in^2	Slope of steady state region, in/min	Shear Strain rate ($\dot{\gamma}$), per second*
523	2.27	8.22×10^{-6}	1.09×10^{-6}
523	10.91	2.66×10^{-5}	3.55×10^{-6}
523	24.5	4.00×10^{-5}	5.005×10^{-6}
523	56.2	9.8×10^{-5}	1.34×10^{-5}
523	179	7.9×10^{-4}	1.04×10^{-4}

* $\dot{\gamma} = \dfrac{\text{Slope}}{\text{Gauge length (1/8 in)} \times 60}$, per second.

Table - VII

Instron Test Data for 1.8μm Grain Size

Temperature, °K	Cross Head Speed, in/min	Shear strain rate ($\dot{\gamma}$), per second*	Shear Stress (τ) lb/in^2
523	2×10^{-4}	2.66×10^{-5}	7.8×10^{1}
523	2×10^{-3}	2.66×10^{-4}	2.6×10^{2}
523	1×10^{-2}	1.33×10^{-3}	6×10^{2}
523	5×10^{-2}	6.66×10^{-3}	1.35×10^{3}
523	1×10^{-1}	1.33×10^{-2}	1.850×10^{3}
523	5×10^{-1}	6.66×10^{-2}	4.4×10^{3}
523	1×10^{0}	1.33×10^{-1}	5.7×10^{3}

* $\dot{\gamma} = \dfrac{\text{Cross Head Speed}}{\text{Grain length (1/8 in)} \times 60}$, per second.

Table - VIII

Creep Test Data for 2.5 μm Grain Size

Temperature °K	Shear Stress (τ), lb/in^2	Slope of Steady state region, in/min.	Shear Strain rate ($\dot{\gamma}$), per second*
522	4.54	5×10^{-6}	6.66×10^{-7}
522	22.6	1.66×10^{-5}	2.2×10^{-6}
522	46.72	4.166×10^{-5}	6.1×10^{-6}
522	89.4	1.2×10^{-4}	1.6×10^{-5}
522	131.5	2.85×10^{-4}	3.8×10^{-5}

* $\dot{\gamma} = \dfrac{\text{Slope}}{\text{Gauge length (1/8 in)} \times 60}$, per second

Table - IX

Instron Test Data for 2.5μm Grain Size

Temperature °K	Cross Head Speed in/min	Shear Strain Rate ($\dot{\gamma}$), per second*	Shear Stress (τ), lb/in^2
522	2×10^{-4}	2.66×10^{-5}	1.01×10^{2}
522	5×10^{-4}	6.66×10^{-5}	1.71×10^{2}
522	1×10^{-3}	1.33×10^{-4}	2.42×10^{2}
522	5×10^{-3}	6.66×10^{-4}	5.25×10^{2}
522	1×10^{-2}	1.33×10^{-3}	7.52×10^{2}
522	1×10^{-1}	1.33×10^{-2}	2.42×10^{3}
522	5×10^{-1}	6.66×10^{-2}	4.505×10^{3}
522	1×10^{0}	1.33×10^{-1}	5.8×10^{3}

* $\dot{\gamma} = \dfrac{\text{Cross Head Speed.}}{\text{Gauge length } (1/8 \text{ in}) \times 60}$, per second.

Table - X

Creep Test Data for 4.8μm Grain Size

Temperature, °K	Shear Stress (τ), lb/in^2	Slope of Steady state region, in/min	Shear strain rate ($\dot{\gamma}$), per second*
523	2.56	4.166×10^{-7}	5.56×10^{-8}
522	11.2	1.25×10^{-6}	1.77×10^{-7}
522	19.2	2.1×10^{-6}	2.8×10^{-7}
522	31.5	5.7×10^{-6}	7.6×10^{-7}
522	56.2	1.35×10^{-5}	1.8×10^{-6}
522	96.4	8.7×10^{-5}	1.16×10^{-5}
522	137.2	9.6×10^{-5}	1.28×10^{-5}
522	185.3	1.9×10^{-4}	2.53×10^{-5}
522	229.2	2.9×10^{-4}	3.86×10^{-5}

* $\dot{\gamma} = \dfrac{\text{Slope}}{\text{Gauge length (1/8 in)} \times 60}$, per second.

Table - XI

Instron Test Data for 4.8μm Grain Size

Temperature, °K	Cross Head Speed, in/min.	Shear strain rate ($\dot{\gamma}$), per second*	Shear Stress (τ), lb/in^2
522	2×10^{-4}	2.66×10^{-5}	2.05×10^{2}
522	2×10^{-3}	2.66×10^{-4}	6.95×10^{2}
522	5×10^{-3}	6.66×10^{-4}	9.82×10^{2}
523	1×10^{-2}	1.33×10^{-3}	1.31×10^{3}
523	5×10^{-2}	6.66×10^{-3}	2.46×10^{3}
523	2×10^{-1}	2.66×10^{-2}	3.92×10^{3}
523	5×10^{-1}	6.66×10^{-2}	6.15×10^{3}

* $\dot{\gamma} = \dfrac{\text{Cross Head Speed.}}{\text{Gauge length (1/8 in) x 60}}$, per second.

Table - XII

Creep Test Data for 5.5 μm Grain Size

Temperature, °K	Shear Stress (τ), lb/in^2	Slope of Steady state region, in/min	Shear Strain Rate ($\dot{\gamma}$) per second*
524	3.32	2.42×10^{-7}	3.225×10^{-8}
524	11.9	7.2×10^{-7}	9.6×10^{-8}
524	19.2	1.1×10^{-6}	1.47×10^{-7}
522	29.2	2×10^{-6}	2.66×10^{-7}
522	42.5	4.3×10^{-6}	5.72×10^{-7}
522	75.2	1.66×10^{-5}	2.2×10^{-6}
522	201	8.6×10^{-5}	1.15×10^{-5}
522	360	2.15×10^{-4}	2.71×10^{-5}

* $\dot{\gamma} = \dfrac{\text{Slope}}{\text{Gauge length (1/8 in)} \times 60}$, per second.

Table - XIII

Instron Test Data for 5.5μm Grain Size

Temperature, °K	Cross Head Speed, in/min	Shear Strain Rate ($\dot{\gamma}$), per second*	Shear stress (τ), lb/in^2
522	2×10^{-4}	2.66×10^{-5}	3.21×10^{2}
522	5×10^{-4}	6.66×10^{-5}	4.52×10^{2}
522	2×10^{-3}	2.66×10^{-4}	9.25×10^{2}
522	2×10^{-2}	2.66×10^{-3}	1.75×10^{3}
522	2×10^{-1}	2.66×10^{-2}	4.102×10^{3}
522	1×10^{0}	1.33×10^{-1}	6.201×10^{3}

* $\dot{\gamma} = \dfrac{\text{Cross Head Speed}}{\text{Gauge length (1/8 in)} \times 60}$, per second.

APPENDIX - V

VALUES OF k, D_g, G AND b USED IN THE CALCULATION OF $\frac{\dot{\gamma} kT}{D_g Gb}$ AND τ/G

$k = 1.38054 \times 10^{-23}$ joules/°K

$G = 4.987 \times 10^{-8}$ psi

$b = 2.5$ Å (Å = 10^{-8} cm)

$D_g = D_o \exp\left(-\frac{\Delta H}{RT}\right)$

$= 0.35 \exp\left(-\frac{16200}{RT}\right)$

$\Delta H \simeq 16.2$ KCal/mol for region I and II

$R = 1.987$ cal/mol.°K.

Substituting we get:

(1) $\frac{\dot{\gamma} kT}{D_g Gb} = 1.0908 \times 10^{-2} \left(e^{16,200/1.987 \times T}\right) \times T \times$ (Slope or Cross Head Speed in in/mt)

(2) $\frac{\tau}{G} = 2.04287 \times 10^{-7} \times$ (Stress in lbs/in^2)

Programme for calculations:

```
1.  10 READ, TEMP, STRESS, SLOPE!
2.  X = 2.04287 E - 07* STRESS!
3.  Y = 1.0908E-20* EXP(16200/(1.987*TEMP)*TEMP*SLOPE!
4.  PRINT, X, Y!
5.  GO TO 10
```

APPENDIX - VI

DATA TABLES FOR $(\frac{\dot{\gamma} kT}{D_g Gb})$ AND (τ/G) FOR VARIOUS GRAIN SIZES AND OTHER PLOTTED DATA

Table - XIV

Calculated Values of $\frac{\dot{\gamma} kT}{D_g Gb}$ and τ/G for Grain Size 1.8/cm

Temp. °K	Stress lb/in^2	Slope in/min.	$\dot{\gamma}$/sec.	τ/G	$\dot{\gamma}$ kT/DGb
523	2.27	8.22×10^{-6}	1.09×10^{-4}	4.6373×10^{-7}	2.7624×10^{-16}
523	10.91	2.66×10^{-5}	3.55×10^{-6}	2.2288×10^{-6}	8.9393×10^{-16}
523	24.5	4×10^{-5}	5.33×10^{-6}	5.005×10^{-6}	1.3442×10^{-15}
523	56.2	9.8×10^{-5}	1.34×10^{-5}	1.1481×10^{-5}	3.2934×10^{-15}
523	179	7.9×10^{-4}	1.05×10^{-4}	3.6567×10^{-5}	2.6549×10^{-14}
523	300	2.34×10^{-3}	3.12×10^{-4}	6.1286×10^{-5}	7.8639×10^{-14}
523	547	9.1×10^{-3}	1.21×10^{-3}	1.1174×10^{-4}	3.0582×10^{-13}
523	1850	1×10^{-1}	1.33×10^{-2}	3.7793×10^{-4}	3.3606×10^{-12}
523	4210	5×10^{-1}	6.66×10^{-2}	8.6005×10^{-4}	1.6803×10^{-11}

Table - XV

Calculated Values of $\frac{\dot{\gamma} kT}{D_g Gb}$ and τ/G

Grain size 2.5μm

Temp. °K	Stress lb/in^2	Slope in/min	$\dot{\gamma}$/sec	τ/G	$\dot{\gamma} kT/D_g Gb$
522	4.54	5×10^{-6}	6.66×10^{-7}	9.2746×10^{-7}	1.7279×10^{-16}
522	22.6	1.66×10^{-5}	2.2×10^{-6}	4.61×10^{-6}	5.7368×10^{-16}
522	46.72	4.166×10^{-5}	6.1×10^{-6}	9.5443×10^{-6}	1.4397×10^{-15}
522	89.4	1.2×10^{-4}	1.6×10^{-5}	1.8263×10^{-5}	4.147×10^{-15}
522	131.5	2.85×10^{-4}	3.8×10^{-5}	2.6864×10^{-5}	9.8493×10^{-15}
522	171	5×10^{-4}	6.66×10^{-5}	3.4933×10^{-5}	1.7279×10^{-14}
522	242	1×10^{-3}	1.33×10^{-4}	4.943×10^{-5}	3.4559×10^{-14}
522	525	5×10^{-3}	6.66×10^{-4}	1.072×10^{-4}	1.7279×10^{-13}
522	752	1×10^{-2}	1.33×10^{-3}	1.5362×10^{-4}	3.4559×10^{-13}
522	2420	1×10^{-1}	1.33×10^{-2}	4.9437×10^{-4}	3.4559×10^{-12}
522	4505	5×10^{-1}	6.66×10^{-2}	9.2031×10^{-4}	1.7279×10^{-11}

Table - XVI

Calculated Values of $\frac{\dot{\gamma} kT}{D_g Gb}$ and τ/G

Grain Size $4\,\mu m$

Temp. °K	Stress lb/in^2	Slope in/min	$\dot{\gamma}$/sec.	τ/G	$\frac{\dot{\gamma} kT}{DGb}$
521	3.32	8.1×10^{-7}	1.08×10^{-7}	6.7823×10^{-7}	2.8789×10^{-17}
521	11.2	1.5×10^{-6}	2×10^{-7}	2.288×10^{-6}	5.3313×10^{-17}
521	31.5	5.9×10^{-6}	7.88×10^{-7}	6.435×10^{-6}	2.097×10^{-16}
521	56.5	1.65×10^{-5}	2.2×10^{-6}	1.1542×10^{-5}	5.8645×10^{-16}
521	96.4	6.4×10^{-5}	8.55×10^{-6}	1.9693×10^{-5}	2.2747×10^{-15}
521	175.2	2.0×10^{-4}	2.66×10^{-5}		7.1085×10^{-15}
521	262.0	5×10^{-4}	6.66×10^{-5}	5.3523×10^{-5}	
521	515	2×10^{-3}	2.66×10^{-4}	1.0521×10^{-4}	7.1085×10^{-14}
521	1160	1×10^{-2}	1.66×10^{-3}	2.3697×10^{-4}	3.5542×10^{-13}
521	1480	2×10^{-2}	2.66×10^{-3}	3.0234×10^{-4}	7.1085×10^{-13}
521	2122	5×10^{-2}	6.66×10^{-3}	4.335×10^{-4}	1.7771×10^{-12}
521	3510	2×10^{-1}	2.66×10^{-2}	7.1705×10^{-4}	7.1085×10^{-12}
521	4542	5×10^{-1}	6.66×10^{-2}	9.2787×10^{-4}	1.7771×10^{-11}

Table - XVII

Calculated Values of $\frac{\dot{\gamma} kT}{D_g Gb}$ and τ/G

for Grain Size 4.8 m

Temp. °K	Stress lb/in^2	Slope in/min	$\dot{\gamma}$/sec	τ/G	$\frac{\dot{\gamma} kT}{DGb}$
523	2.56	4.166×10^{-7}	5.56×10^{-8}	5.229×10^{-7}	1.4×10^{-17}
522	11.2	1.25×10^{-6}	1.77×10^{-7}	2.288×10^{-6}	4.3198×10^{-17}
522	19.2	2.1×10^{-6}	2.8×10^{-7}	3.922×10^{-6}	7.257×10^{-17}
522	31.5	5.7×10^{-6}	7.6×10^{-7}	6.435×10^{-6}	1.9699×10^{-17}
522	35.6	6.0×10^{-6}	8×10^{-7}	7.2726×10^{-6}	2.0735×10^{-16}
522	56.2	1.35×10^{-5}	1.8×10^{-6}	1.1481×10^{-5}	4.6654×10^{-16}
522	96.4	8.7×10^{-5}	1.16×10^{-5}	1.9693×10^{-5}	3.0066×10^{-15}
522	137.2	9.6×10^{-5}	1.28×10^{-5}	2.8028×10^{-5}	3.3176×10^{-15}
522	185.3	1.9×10^{-4}	2.53×10^{-5}	3.785×10^{-5}	6.5662×10^{-15}
522	229.2	2.9×10^{-4}	3.86×10^{-5}	4.6823×10^{-5}	1.0022×10^{-14}
522	205	2×10^{-4}	2.66×10^{-5}	4.1879×10^{-5}	6.9118×10^{-15}
522	695	2×10^{-3}	2.66×10^{-4}	1.4198×10^{-4}	6.9118×10^{-14}
522	982	5×10^{-3}	6.66×10^{-4}	2.0061×10^{-4}	1.7279×10^{-13}
522	1310	1×10^{-2}	1.66×10^{-3}	2.6762×10^{-4}	3.4559×10^{-13}
522	1702	2×10^{-2}	2.66×10^{-3}	$3.47\ 7 \times 10^{-4}$	6.9118×10^{-13}
522	2460	5×10^{-2}	6.66×10^{-3}	5.0255×10^{-4}	1.7279×10^{-12}
522	3920	2×10^{-1}	2.66×10^{-2}	8.0081×10^{-4}	6.9118×10^{-12}
522	6150	5×10^{-1}	6.66×10^{-2}	1.25637×10^{-3}	1.7279×10^{-11}

Table - XVIII

Calculated values of $\frac{\dot{\gamma} kT}{D_g Gb}$ and τ/G

for Grain Size 5.5 m

Temp. °K.	Stress lb/in^2	Slope in/min	$\dot{\gamma}$/sec.	τ/G	$\dot{\gamma} kT/D_g Gb$
524	3.32	2.42×10^{-7}	3.225×10^{-8}	6.7828×10^{-7}	7.9094×10^{-18}
524	11.9	7.2×10^{-7}	9.6×10^{-8}	2.431×10^{-6}	2.3532×10^{-17}
524	19.2	1.1×10^{-6}	1.47×10^{-7}	3.9223×10^{-6}	3.5952×10^{-17}
522	29.2	2×10^{-6}	2.66×10^{-7}	5.9652×10^{-6}	6.9118×10^{-17}
522	42.5	4.3×10^{-6}	5.72×10^{-7}	8.6822×10^{-6}	1.486×10^{-16}
522	75.2	1.66×10^{-5}	2.2×10^{-6}	1.5362×10^{-5}	5.7368×10^{-16}
522	201	8.6×10^{-5}	1.15×10^{-5}	4.1062×10^{-5}	2.9721×10^{-15}
522	321	2×10^{-4}	2.66×10^{-5}	6.5576×10^{-5}	6.9118×10^{-15}
522	452	5×10^{-4}	6.66×10^{-5}	9.2338×10^{-5}	1.7279×10^{-15}
522	925	2×10^{-3}	2.66×10^{-4}	1.8897×10^{-4}	6.9118×10^{-14}
522	1750	2×10^{-2}	2.66×10^{-3}	3.575×10^{-4}	6.9118×10^{-13}
522	4102	2×10^{-1}	2.66×10^{-2}	8.3799×10^{-4}	6.9118×10^{-12}
522	6201	1	1.66×10^{-1}	1.26678×10^{-3}	3.4559×10^{-11}

Table - XIX

Instron Data at Various Temperatures for d=1.8μm

	250°C	225°C	200°C	175°C
CHS	Stress, lb/in^2	stress, lb/in^2	stress, lb/in^2	stress, lb/in^2
.0002	7.8×10^1	1.5×10^2	2.4×10^2	3.7×10^2
.002	2.6×10^2	4.5×10^2	7.1×10^2	1.12×10^3
.01	6×10^2	1.05×10^3	1.48×10^3	2.5×10^3
.05	1.35×10^3	2.35×10^3	3.36×10^3	5.1×10^3
.1	1.85×10^3	3.1×10^3	4.5×10^3	6.7×10^3
.5	4.4×10^3	6.2×10^3	9.05×10^3	1.07×10^4
1	5.7×10^3	-	-	-
2	-	9×10^3	1.2×10^4	1.55×10^4

Table - XX

Instron Data at various Temperatures for d=4μm

CHS	250°C stress, lb/in^2	225°C stress, lb/in^2	200°C stress, lb/in^2	175°C stress, lb/in^2
.0002	1.45×10^2	2.3×10^2	4×10^2	6.05×10^2
.0005	-	3.7×10^2	6.1×10^2	9.02×10^2
.002	4.6×10^2	7.1×10^2	1.2×10^3	1.8×10^3
.01	1×10^3	1.45×10^3	2.5×10^3	3.4×10^3
.02	1.3×10^3	2×10^3	3.1×10^3	4.2×10^3
.05	1.8×10^3	2.8×10^3	-	5.6×10^3
.2	3.5×10^3	4.7×10^3	6.5×10^3	8.5×10^3
1	5.7×10^3	8.45×10^3	1.25×10^4	1.44×10^4

Table - XXI

Instron Data at Various Temperatures for d=5.5μm

CHS	250°C Stress lb/in^2	225°C Stress lb/in^2	200°C Stress lb/in^2	175°C Stress lb/in^2
.0002	3.4×10^2	5.4×10^2	9.6×10^2	1.7×10^3
.0005	4.5×10^2	8×10^2	1.5×10^3	2.6×10^3
.002	9.4×10^2	1.6×10^3	2.5×10^3	4×10^3
.02	1.9×10^3	3×10^3	4.9×10^3	7.96×10^3
.2	4×10^3	6×10^3	1×10^4	1.5×10^4
1	6.5×10^3	9.6×10^3	1.48×10^4	2.5×10^4
2	7.98×10^3	1.2×10^4	1.9×10^4	2.98×10^4

Table - XXII

Data for Graphs in Figure 35

Grain size 4μm

Temperature	Slope (in/mt)	
250°C	1.25×10^{-6}	
225°C	4.8×10^{-7}	$\tau = 5$ lb/in^2, d = 4μm.
200°C	1.8×10^{-7}	
175°C	7.4×10^{-8}	
	Grain size 2.5 m	
250°C	7.4×10^{-6}	
225°C	2.8×10^{-6}	$\tau = 8$ lb/in^2, d = 2.5μm.
200°C	1.2×10^{-6}	
175°C	4.1×10^{-7}	

Table - XXIII

Data for Graphs in Figure 36

Grain size 1.8μm and $\tau = 6 \times 10^2$

Temperature	Cross-head Speed in/mt. (or Slope)
250°C	1×10^{-2}
225°C	3.65×10^{-3}
200°C	1.5×10^{-3}
175°C	5×10^{-4}
Grain size 4μm and $\tau = 7 \times 10^2$	
250°C	3.8×10^{-3}
225°C	1.5×10^{-3}
200°C	5.4×10^{-4}
175°C	2.1×10^{-4}

Table - XXIV

Data for Graph in Figure 37

Grain size 5.5μm

$\tau = 7.98 \times 10^3$ lb/in^2

Temperature	Cross-head speed in/mt.
250°C	2
225°C	0.5
200°C	0.1
175°C	0.020